PHYSICAL REVIEW B VOLUME 50, NUMBER 17 1 NOVEMBER 1994-I

# Temperature derivative of the superfluid density and flux quantization as criteria for superconductivity in two-dimensional Hubbard models

F.F. Assaad* and W. Hanke
*Physikalisches Institut, Universität Würzburg, 97074 Würzburg, Federal Republic of Germany*

D.J. Scalapino
*Department of Physics, University of California, Santa Barbara, California 93106-9530*
(Received 28 March 1994; revised manuscript received 11 July 1994)

Based on extensions of quantum Monte Carlo algorithms to incorporate magnetic fields, two criteria to detect superconductivity in two-dimensional Hubbard models are investigated. In order to provide such criteria, we calculate both the internal energy $E(\Phi,T)$ as well as the ground-state energy, $E_0(\Phi)$, for Hubbard models on a cylinder geometry threaded by a flux $\Phi$. The temperature derivative of the superfluid density, $\partial\beta D_s(\beta)/\partial\beta$, is obtained from the difference in internal energy of systems which differ by a phase twist $\pi/2$ in the boundary condition along one lattice direction. In the framework of a Kosterlitz-Thouless transition, $\partial\beta D_s(\beta)/\partial\beta$ scales to a Dirac $\delta$ function at the transition temperature. On finite-sized lattices, $\partial\beta D_s(\beta)/\partial\beta$ shows a response which increases with lattice size. Flux quantization is a $T=0$ method. From the functional form of $E_0(\Phi)$, superconducting or nonsuperconducting ground states may be identified. In both approaches, superconductivity may be detected without prior knowledge of the symmetry and nature of the pairing correlations. For single-band Hubbard models, our main quantum Monte Carlo results include numerical data which (a) confirm the existence and pin down the transition temperature of a Kosterlitz-Thouless-type transition in the attractive Hubbard model away from half-band filling and (b) show that the quarter-filled repulsive Hubbard model is not superconducting. For the three-band Hubbard model we consider two parameter sets which take into account the differences in static magnetic structure and Fermi surfaces between La-Sr-Cu-O and Y-Ba-Cu-O materials. For both parameter sets, the finite-temperature approach showed no sign of a Kosterlitz-Thouless-type transition up to inverse temperatures $\beta = 17.5$, in units of the Cu-O hopping, and hole doping $\delta = 0.25$. Flux quantization results for the Y-Ba-Cu-O parameters on clusters up to $8 \times 8$ unit cells equally showed no sign of superconductivity at a hole doping $\delta = 0.25$.

## I. INTRODUCTION

Despite tremendous efforts in conjunction with theoretical studies of high-$T_c$ superconductivity in the last years, the question of whether two-dimensional repulsive Hubbard-type models[1,2] have, in addition to metallic and insulating phases, a superconducting ground state is still unresolved. Apart from approximative approaches,[3,4] state-of-the-art numerical methods have been applied. In particular, with the quantum Monte Carlo (QMC) method, pairing correlations in different symmetry channels (e.g., extended $s$ wave, $d_{x^2-y^2}$) have been calculated.[5–7] Although in some cases an attractive interaction was established, the issue of the existence of off-diagonal long-range order (ODLRO) required for a superconducting ground state is still unresolved. The major reason for this failure lies in the difficulty of reaching low enough temperatures due to the onset of the sign problem away from half band filling. Apart from this problem, assumptions made on the symmetry and nature (i.e., for example, leaving out retardation effects) may have prevented the discovery of a superconducting ground state.

In this paper, on the basis of QMC simulations, we test and apply two methods to detect superconductivity without any prior knowledge of the symmetry of the underlying pairing correlations. In order to provide such criteria for superconductivity, we calculate both the internal energy $E(\Phi,T)$, as well as the ground-state energy $E_0(\Phi)$, for Hubbard models on a cylinder geometry threaded by a flux $\Phi$. The technical innovation we introduce is a generalization of standard QMC algorithms[8,6,9–11] to incorporate magnetic fields. The strong point of the $T=0$ and finite-$T$ methods is that they rely only on the calculation of the energy for a given flux $\Phi$. This quantity is the most stable observable obtained from QMC simulations. This allows us to carry out accurate simulations up to average signs of the order of 0.1.

Our finite-temperature approach is based on the calculation of the temperature derivative of the superfluid density, $\frac{\partial\beta D_s(\beta)}{\partial\beta}$. As we will see, the latter quantity is given by the difference in internal energies of systems which differ by a phase twist $\pi/2$ in the boundary condition along one lattice direction. This $\pi/2$ phase twist is equivalent to threading a flux $\Phi = \Phi_0/4$ ($\Phi_0 = hc/e$) through a cylinder on which lies the electronic system. The internal energies are extracted from the grand-canonical finite-temperature QMC algorithm on finite-sized cluster. In the framework of the Kosterlitz-Thouless[12] (KT) transition, $D_s(\beta)$ shows a universal jump at the tran-

 ©1994 The American Physical Society

sition temperature.[13] Hence, $\frac{\partial \beta D_s(\beta)}{\partial \beta}$ in the thermodynamic limit behaves like a Dirac $\delta$ function at the transition temperature $T_{\rm KT}$ and even on finite-sized clusters is expected to yield a peak at $T_{\rm KT}$ which grows as the size of the system increases. This provides a clear signal of the KT transition. Such signatures of the KT transition have already been observed in classical[14] as well as in quantum $XY$ models.[15]

A second method we use as a numerical criterion for ODLRO in two-dimensional Hubbard models is flux quantization. It is a $T = 0$ approach which is based on the projector QMC (PQMC) algorithm. The setup of the numerical experiment we carried out is the following. We place the electronic system on a cylinder. Through the cylinder, we thread a flux $\Phi$ and calculate with the PQMC the ground-state energy as a function of the threaded flux, $E_0(\Phi)$. From the functional form of $E_0(\Phi)$, one may distinguish between normal and superconducting ground states. In the case of a superconductor (i.e., off-diagonal long-range order), Byers and Yang[16,17] have argued that $E_0(\Phi)$ is a periodic function of $\Phi$ with period $\Phi_0/n$. Here, $n$ stands (in Yang's notation[17]) for the sum of charges of the particles in the basic group ($n = 2$ for Cooper pairs and $n = m$ for a Bose condensation of charge $m$ bosons), and $\Phi_0 = hc/e$. Furthermore, a nonvanishing energy barrier is to be found between the flux minima. This picture stands in close relationship to the existence of persistent currents[18] since supercurrents are trapped in metasable states corresponding to flux minima and thus cannot *dribble* away.[19] On the other hand, the curve $E_0(\Phi)$ is expected to be flat in the case of a crystal in its normal phase. Here, we emphasize that the above discussion is valid in the thermodynamic limit. Hence, $E_0(\Phi)$ has to be calculated on several lattice sizes so as to try to extrapolate to the thermodynamic limit. Flux quantization studies based on the Lanczos algorithm for the two-dimensional $t$-$J$ model have been carried out by Dagotto and Riera.[20] However, as pointed out by the authors, due to the restrictions on lattice size inherent to the Lanczos algorithm, their results show pairing but not ODLRO for the quarter-filled $t$-$J$ model at $J/t = 3$. In one dimension exact diagonalization studies of flux quantization have been carried out by Sudbø *et al.*[21] for copper oxide chains. Clearly, in one dimension, no ODLRO exists, and there is no Meisner effect. Let us stress that our flux quantization calculations for two-dimensional Hubbard models are based on the PQMC algorithm which allows us, to a certain extent, to carry out simulations on several lattice sizes. For the three-band Hubbard model, simulations up to $8 \times 8$ unit cells (i.e., 192 sites) were carried out.

Recently, Scalapino *et. al.*[22] have measured with QMC methods the finite-temperature linear response of the attractive and repulsive Hubbard models to a transverse magnetic field of wave vector $\mathbf{q}$. By taking the limit $\mathbf{q} \to 0$, which implicitly requires the system size to diverge, they obtain the superfluid density. Clearly, this approach also detects superconducting phases without prior knowledge of the symmetry of the underlying pair correlations. Since the superfluid density may be obtained from our $E_0(\Phi)$ data,[17,22] both methods are complementary, and as we shall see, yield comparable results.

The paper is organized as follows. In Sec. II the technical aspects of the projector QMC (PQMC) and grand-canonical QMC algorithms are described. The technical innovation is the presence of a vector potential which accounts for the threaded flux. This forces us to work with complex numbers. Apart from multiplying the CPU time by a factor of 3—4, the major consequence of working with complex numbers is that the sign problem is replaced by a phase problem. We discuss in detail the phase problem (Sec. II B), as well as the systematic error which occurs in QMC algorithms due to the Trotter decomposition of the imaginary time propagator (Sec. II C). Concerning the systematic error produce by the Trotter decomposition, Fye[23] has shown that even when the lowest-order Trotter decomposition is used, the systematic error is proportional to $(\Delta\tau)^2$ provided that the relevant operators are simultaneously real representable. Here, $\Delta\tau$ denotes the imaginary time step. The above assumption is valid for Hubbard models. However, when a magnetic field is introduced it is not necessarily valid. For completeness sake, we consider in Sec. II D a model of interacting spinless fermions in a transverse magnetic field. For this model, the above assumption of simultaneous real representability is no longer valid and an alternative algorithm based on a higher-order Trotter decomposition is presented.

In Sec. III we present results on flux quantization for the attractive and repulsive Hubbard models. The method is first *tested* on the attractive Hubbard model. The major result of this section is numerical evidence showing that the quarter-filled repulsive Hubbard model displays no superconductivity at $T = 0$. Section IV summarizes our results on the temperature derivative of the superfluid density. The results presented give clear numerical evidence for the occurrence of a KT-type transition away from half band filling for the attractive Hubbard model.

In Sec. V we turn to the three-band Hubbard model. For this model, we use both above described criteria to detect superconductivity. We consider two parameter sets which reproduce the observed differences in static magnetic structure between La-Sr-Cu-O and Y-Ba-Cu-O materials.[28,29] The free Fermi surface of our two parameter sets reproduce to a certain extent the local-density-approximation (LDA) Fermi surfaces of both materials.[24–26] The relation between the form of the Fermi surface and magnetic structure has recently been emphasized by Si *et al.*[27] For our La-Sr-Cu-O parameter set, no sign of a KT transition was found on $4 \times 4$ ($6 \times 6$) lattices up to temperatures of $\beta t_{pd} = 17.5$ ($\beta t_{pd} = 12.5$) at a hole doping $\delta = 0.25$. Here, $t_{pd}$ denotes the hopping matrix element between the Cu $d_{x^2-y^2}$ and the O $p_{x,y}$ orbitals. For the Y-Ba-Cu-O parameters, our simulations on $4 \times 4$ lattices at $\delta = 0.25$ also showed no sign of a KT transition up to $\beta t_{pd} = 17.5$. For the latter parameter set, we present $T = 0$ flux quantization data for various lattices sizes up to $8 \times 8$ which again show no sign of superconductivity at $\delta = 0.25$.

Finally, in Sec. VI conclusions are drawn.

## II. QUANTUM MONTE CARLO ALGORITHMS AND MAGNETIC FIELDS

In this section, we discuss the projector quantum Monte Carlo (PQMC) algorithm applied to electronic systems in a magnetic field. The core of the algorithm is identical to the standard PQMC algorithm[8] which is described in detail in Ref. 11. The presence of a vector potential forces us to work with complex numbers. Apart from enhancing the CPU time by a factor of 3–4 the major consequence of working with complex numbers is that the sign problem is replaced by a phase problem. As we will see, working with complex numbers does not complicate the algorithms, and adds a set of cross-checks for the quality of the sampling. This section is organized as follows. We describe below briefly the PQMC algorithm. We will then in Secs. II B and II C discuss respectively the phase problem and the systematic error produced by the discretization of the imaginary time propagator. In Secs. II B and II C we consider vector potentials of the form $\mathbf{A} = \Phi \mathbf{e}_1/L$ where $L$ denotes the linear length of the square lattice. These vector potentials twist the $\mathbf{e}_1$ boundary condition by a phase factor $\exp(2\pi i\Phi/\Phi_0)$. Hence, for the models we will consider (attractive, repulsive, and three-band Hubbard models), the Hamiltonian is real representable in Fourier space. The assumption that the relevant operators are simultaneously real representable is very useful for the PQMC algorithm. For completeness, we consider in Sec. II D a model of spinless fermions in a static transverse magnetic field. For this model the above assumption is not necessarily valid, and we present an alternative algorithm based on a higher-order Trotter decomposition. In Sec. II E, we briefly mention the finite-temperature QMC algorithm[9,10] since our results of Sec. IV are based on this algorithm. The finite-temperature algorithm reacts in exactly the same way as the PQMC algorithm to the presence of a magnetic field.

### A. PQMC algorithm

The Hamiltonians we consider are of the form

$$H = -t \sum_{\langle \mathbf{i},\mathbf{j}\rangle,\sigma} c^{\dagger}_{\mathbf{i},\sigma} c_{\mathbf{j},\sigma} \exp\left(\frac{2\pi i}{\Phi_0}\int_{\mathbf{i}}^{\mathbf{j}} \mathbf{A} d\mathbf{l}\right) + V. \quad (1)$$

Here, $c^{\dagger}_{\mathbf{i},\sigma}$ creates an electron with a $z$ component of spin $\sigma$ on lattice site $\mathbf{i}$, $\Phi_0 = he/c$ is the flux quantum, $\mathbf{A}$ denotes the vector potential, $V$ corresponds to a density-density type interaction, and the sum runs over nearest neighbors of the underlying square lattice. The PQMC algorithm yields the ground-state expectation value of an observable $O$ in the canonical ensemble and is based on the following equation:

$$\frac{\langle\Psi_0|O|\Psi_0\rangle}{\langle\Psi_0|\Psi_0\rangle} = \lim_{\Theta\to\infty} \frac{\langle\Psi_T|e^{-\Theta H/2} O e^{-\Theta H/2}|\Psi_T\rangle}{\langle\Psi_T|e^{-\Theta H}|\Psi_T\rangle}, \quad (2)$$

where $|\Psi_T\rangle$ is a Slater determinant which is required to be nonorthogonal to the ground state $|\Psi_0\rangle$.

Through the use of the Trotter formula, we approximate the imaginary time propagator $e^{-\Theta H}$ by[23]

$$\left(e^{-\Delta\tau K} e^{-\Delta\tau V}\right)^m = e^{-\Theta H} + \frac{\Delta\tau}{2}\int_0^{\Theta} d\tau e^{-(\Theta-\tau)H} \times [K,V] e^{-\tau H} + O((\Delta\tau)^2). \quad (3)$$

Here, $\Delta\tau m = \Theta$ and $H = K + V$. We have explicitly included the first-order correction in $\Delta\tau$ since in the presence of a magnetic field it does not necessarily vanish (see Sec. II D). We introduce the notation $H_1(\Theta) = \int_0^{\Theta} d\tau e^{-(\Theta-\tau)H}[K,V]e^{-\tau H}$ and $B(\Theta) = \left(e^{-\Delta\tau K}e^{-\Delta\tau V}\right)^m$, with $m\Delta\tau = \Theta$. One may then write Eq. (2) as

$$\frac{\langle\Psi_T|e^{-\Theta H/2} O e^{-\Theta H/2}|\Psi_T\rangle}{\langle\Psi_T|e^{-\Theta H}|\Psi_T\rangle} = \langle O\rangle_{\text{approx}} - \frac{\Delta\tau}{2}\frac{\langle\Psi_T|A_1|\Psi_T\rangle}{\langle\Psi_T|B(\Theta)|\Psi_T\rangle} + O((\Delta\tau)^2),$$

where

$$A_1 = B(\Theta/2) O H_1(\Theta/2) + H_1(\Theta/2) O B(\Theta/2) - \langle O\rangle_{\text{approx}} H_1(\Theta)$$

$$\langle O\rangle_{\text{approx}} = \frac{\langle\Psi_T|B(\Theta/2)OB(\Theta/2)|\Psi_T\rangle}{\langle\Psi_T|B(\Theta)|\Psi_T\rangle}. \quad (4)$$

We will now consider the Monte Carlo evaluation of $\langle O\rangle_{\text{approx}}$ and will later on come back to the systematic error produced by finite values of $\Delta\tau$. For the models we consider (attractive, repulsive, and three-band Hubbard Hamiltonians), one may carry out a discrete Hubbard-Stratonovich (HS) decoupling of the two-body interaction term,[30]

$$\exp(-\Delta\tau V) = \sum_{\mathbf{s}} \exp\left(\sum_{x,y} c^{\dagger}_x D_{x,y}(\mathbf{s}) c_y\right). \quad (5)$$

Here, $\mathbf{s}$ denotes a vector of HS Ising fields and $x$ labels a single-particle state (i.e., spin and lattice site). As mentioned previously, the trial wave function is a Slater determinant and may be written in the form

$$|\Psi_T\rangle = \prod_{n=1}^{N_p}\left(\sum_x c^{\dagger}_x P_{x,n}\right)|0\rangle. \quad (6)$$

$N_p$ denotes the number of particles and $P$ is a $N_s \times N_p$ rectangular matrix where $N_s$ is the number of single-particle states. Combining Eqs. (5) and (6) yields

$$\langle\Psi_T|B(\Theta)|\Psi_T\rangle = \sum_{\mathbf{s}} \det M(\mathbf{s}),$$

where

$$M(\mathbf{s}) = U^L(\tau,\mathbf{s}) U^R(\tau,\mathbf{s}),$$

$$U^L(\tau,\mathbf{s}) = P^{\dagger}\prod_{n=m}^{\tau+1}\left(e^{-\Delta\tau T} e^{D(\mathbf{s}_n)}\right),$$

$$U^R(\tau,\mathbf{s}) = \prod_{n=1}^{\tau}\left(e^{-\Delta\tau T} e^{D(\mathbf{s}_n)}\right) P. \quad (7)$$

In the above equation, the matrix $T$ contains the hopping matrix elements (i.e., $K = \sum_{x,y} c_x^\dagger T_{x,y} c_y$). Note that the matrix $M(\mathbf{s})$ is independent of $\tau$. Observables may be calculated with

$$\langle O \rangle_{\text{approx}} = \frac{\sum_{\mathbf{s}} \det(M(\mathbf{s})) \langle\langle O \rangle\rangle(\tau, \mathbf{s})}{\sum_{\mathbf{s}} \det[M(\mathbf{s})]}, \tag{8}$$

where $\langle\langle O \rangle\rangle(\tau, \mathbf{s})$ denotes the expectation value of the observable O for a given HS configuration $\mathbf{s}$ and on time slice $\tau$. As for the calculation of $\langle\langle O \rangle\rangle(\tau, \mathbf{s})$, one notes that for a fixed HS configuration of Ising spins, one has a free theory interacting with the HS field. Thus, Wick's theorem holds and $\langle\langle O \rangle\rangle(\tau, \mathbf{s})$ is given by its Wick's reduction. Hence it suffices to calculate the Green functions. They are given by

$$\langle\langle c_x^\dagger c_y \rangle\rangle(\tau, \mathbf{s}) = \left\{ U^R(\tau, \mathbf{s}) \left[ U^L(\tau, \mathbf{s}) U^R(\tau, \mathbf{s}) \right]^{-1} U^L(\tau, \mathbf{s}) \right\}_{y,x}. \tag{9}$$

Provided that $\det[M(\mathbf{s})]$ is positive, one may evaluate $\langle O \rangle_{\text{approx}}$ through a Monte Carlo importance sampling of the probability distribution $P(\mathbf{s}) = \det[M(\mathbf{s})] / \sum_{\mathbf{s}} \det[M(\mathbf{s})]$. Unfortunately, $\det[M(\mathbf{s})]$ is not necessarily positive definite and hence $P(\mathbf{s})$ may not be interpreted as a probability distribution. This gives rise to the sign or, in our case, the phase problem. When $\det[M(\mathbf{s})]$ is not positive, one defines an auxiliary probability distribution

$$P_a(\mathbf{s}) = \frac{|\det[M(\mathbf{s})]|}{\sum_{\mathbf{s}} |\det[M(\mathbf{s})]|}, \tag{10}$$

with which the Monte Carlo sampling is carried out. Observables are then calculated via

$$\langle O \rangle_{\text{approx}} = \frac{\sum_{\mathbf{s}} P_a(\mathbf{s}) \text{Ph}(\mathbf{s}) \langle\langle O \rangle\rangle(\mathbf{s})}{\sum_{\mathbf{s}} P_a(\mathbf{s}) \text{Ph}(\mathbf{s})},$$

where

$$\text{Ph}(\mathbf{s}) = \frac{\det[M(\mathbf{s})]}{|\det[M(\mathbf{s})]|}. \tag{11}$$

### B. Phase problem

Retracing our steps, one may see that the average phase is given by

$$\langle \text{Ph} \rangle = \sum_{\mathbf{s}} P_a(\mathbf{s}) \text{Ph}(\mathbf{s}) = \frac{\langle \Psi_T | B(\Theta) | \Psi_T \rangle}{\sum_{\mathbf{s}} |\det[M(\mathbf{s})]|}, \tag{12}$$

where $B(\Theta)$ was defined by $\left( e^{-\Delta\tau K} e^{-\Delta\tau V} \right)^m$. In the limit $\Delta\tau \to 0$, $m \to \infty$, and $m\Delta\tau = \Theta$, $B(\Theta)$ scales to $\exp(-\Theta H)$. Since $H$ is Hermitian, $\langle \Psi_T | \exp(-\Theta H) | \Psi_T \rangle$ is real and the average phase is a real quantity. On the other hand, for finite values of $\Delta\tau$, $B(\Theta)$ is not Hermitian and thus the average phase is not necessarily real. However, for the models and vector potentials we considered, $V = \pm U \sum_i n_{i,\uparrow} n_{i,\downarrow}$ and $\mathbf{A} = \Phi \mathbf{e}_1 / L$, both $K$ and $V$ are simultaneously real representable in Fourier space. Furthermore, the trial wave function $|\Psi_T\rangle$ was chosen as the ground state of the noninteracting Hamiltonian. For all our calculations, we have chosen this trial wave function. Under those circumstances, one may show that $\langle \Psi_T | B(\Theta) | \Psi_T \rangle$ is a real number. Hence the average phase is real. In the same way, one may show that for finite values of $\Delta\tau$, $\langle O \rangle_{\text{approx}}$ [Eq. (4)] is real provided that $K$, $V$, $O$, and $|\Psi_T\rangle$ are simultaneously real representable. This condition is clearly satisfied for $O = H$ and the above mentioned choice of the trial wave function. Note that for a given HS configuration both the phase and energy are not real. Thus, the Monte Carlo sampling is responsible for the cancellation of the imaginary part of the phase and energy. This provides a good test for the ergodicity of the sampling.

As an example, we consider the attractive Hubbard model. Figure 1(a) plots the imaginary and real parts of

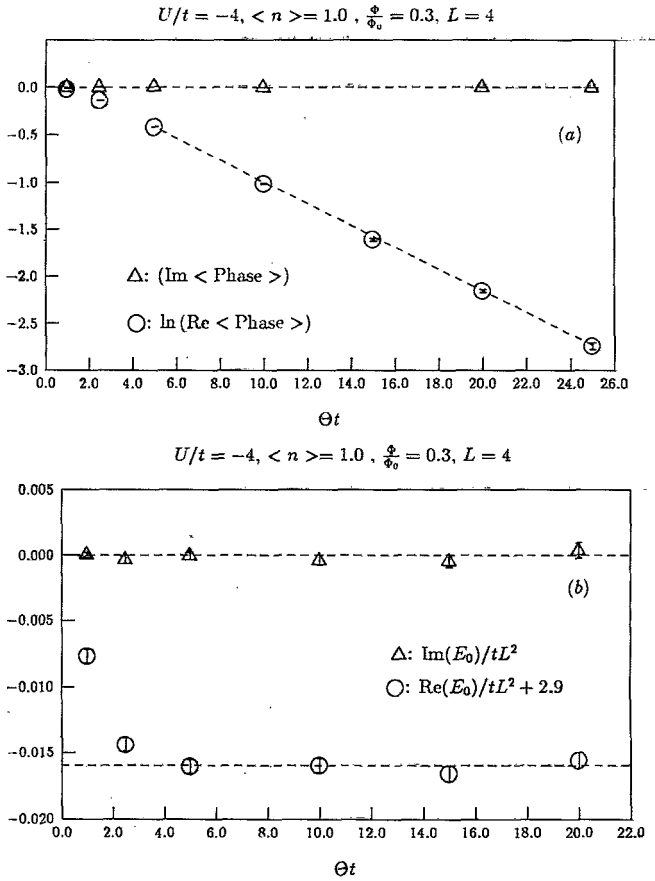


FIG. 1. (a) Imaginary and real parts of the average phase as a function of the projection parameter $\Theta$ for the half-filled attractive Hubbard model at $U/t = -4$, $\mathbf{A} = 0.3\Phi_0 \mathbf{e}_1 / L$, and for a $4 \times 4$ lattice. The trial wave function was chosen as the ground state of the noninteracting part of the Hamiltonian and $\Delta\tau t = 0.125$. (b) Real and imaginary parts of the energy as a function of the projection parameter $\Theta$ for the same model and parameters as in (a).

the average phase for the half-filled attractive Hubbard model at $U/t = -4$, and for the vector potential $\mathbf{A} = 0.3\Phi_0\mathbf{e}_1/L$ as a function of the projection parameter $\Theta$.[31] One may see that the imaginary part of the phase is zero within out error bars, and that the real part of the phase decays exponentially with growing values of the projection parameter $\Theta$. Thus, the real part of the phase plays the role of the average sign in real number QMC simulations.

Since the average phase scales exponentially to zero with growing projection parameter $\Theta$, observables are strictly speaking given by the quotient of two vanishing quantities (4). However, for a given statistical uncertainty, finite values of $\Theta$ are required to filter out the ground state from the trial wave function. Figure 1(b) plots the *imaginary* and real parts of the energy again for the half-filled attractive Hubbard model at $U/t = -4$, and for the vector potential $\mathbf{A} = 0.3\Phi_0\mathbf{e}_1/L$ as a function of the projection parameter $\Theta$. One may see that the imaginary part of the energy vanishes within our error bars and that values of $\Theta t \sim 10$ are sufficient to filter out the ground-state energy from the trial wave function. We have carried out most of our calculations at $\Theta t = 10$.

Figure 2 plots the real part of the average phase as a function of $\Phi/\Phi_0$ for the vector potential $\mathbf{A} = \Phi\mathbf{e}_1/L$ and for the half-filled attractive (a) and quarter-filled repulsive (b) Hubbard models. Apart from special points where the average phase is identical to 1, the variation of the average phase may be traced back to the creation and annihilation of filled shell configurations (i.e., the ground state of the noninteracting system is nondegenerate). Consider the $8 \times 8$ lattice for the quarter-filled repulsive Hubbard model. For this filling and antiperiodic (periodic) boundary conditions in the $\mathbf{e}_1$ ($\mathbf{e}_2$) direction (i.e., $\Phi/\Phi_0 = 0.5$), one has a filled shell configuration and the average phase is approximately equal to 1. As $\Phi/\Phi_0$ is lowered, the gap [i.e, $E(N+1) - 2E(N) + E(N-1)$ where $E(N)$ denotes the ground-state energy of the noninteracting system with $N$ particles] decreases as does the average phase.

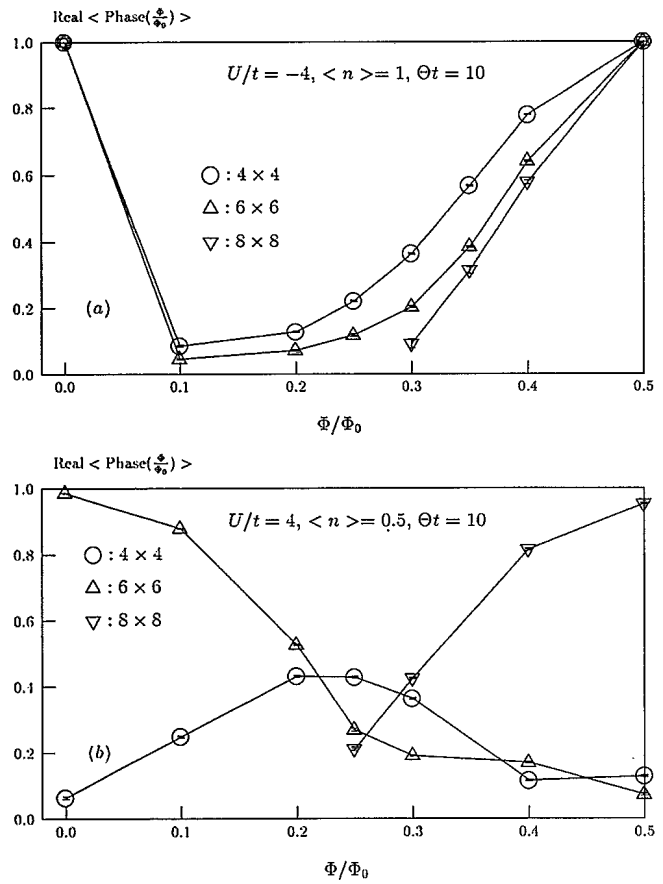


FIG. 2. (a) Real part of the average phase as a function of $\Phi/\Phi_0$ ( $\mathbf{A} = \Phi\mathbf{e}_1/L$ ) for the half-filled attractive Hubbard model at $U/t = -4$. The trial wave function was chosen as the ground state of the noninteracting part of the Hamiltonian and $\Delta\tau t = 0.125$. (b) Same as (a) but for the quarter-filled repulsive Hubbard Hamiltonian at $U/t = 4$.

### C. $\Delta\tau$ systematic error

The systematic error produced by a finite value of $\Delta\tau$ is at first glance proportional to $\Delta\tau$ [see Eq. (4)). However, under the assumption that $O$, $K$, $V$, and $|\Psi_T\rangle$ are simultaneously real representable, the prefactor of the systematic error proportional to $\Delta\tau$ vanishes.[23] This may be shown by noting that (i) $H_1(\Theta)$ is antihermitian, (ii) $\langle O\rangle_{\text{approx}}$ is real, and hence (iii) $A_1$ [see Eq. (4)] is anti-Hermitian and real representable. It then follows that $\langle\Psi_T|A_1|\Psi_T\rangle = 0$ and the systematic error produced by finite values of $\Delta\tau$ is proportional to $(\Delta\tau)^2$.[32]

Figure 3 plots the ground-state energy as a function of $\Delta\tau$ for the attractive and repulsive half-filled Hubbard models. Note that at half-filling, with $H = -t\sum_{\langle\mathbf{i},\mathbf{j}\rangle,\sigma} c^\dagger_{\mathbf{i},\sigma}c_{\mathbf{j},\sigma} + U\sum_{\mathbf{i}} n_{\mathbf{i},\uparrow}n_{\mathbf{i},\downarrow}$ and periodic bounbary conditions, $[E_0(U) - E_0(-U)]/tL^2 = U/2t$. Here, we consider the vector potential $\mathbf{A} = \Phi\mathbf{e}_1/L$ for different values of $\Phi$. The projection parameter was set to $\Theta t = 10$ and the trial wave function was chosen as the ground state of the noninteracting system. As mentioned previously, for the considered models and vector potentials, all relevant operators are simultaneously real representable. As expected, one may see from Fig. 3 that in all cases, the $\Delta\tau$ systematic error scales as $(\Delta\tau)^2$. We furthermore wish to mention that (i) for $\Phi/\Phi_0 = 0$ and both considered models, our QMC data scale to the exact diagonalization value of the energy. This confirms that values of $\Theta t = 10$ are sufficient to filter out the ground state from the trial wave function. (ii) Energy differences at different values of the flux $\Phi$ are to a very good approximation independent of $\Delta\tau$. This is crucial, since all our results are extracted from energy differences at different values of the flux $\Phi$. Hence, we believe that our results are to a good approximation not plagued by systematic error arising from finite values of $\Delta\tau$. For all our simulations we have set $\Delta\tau t = 0.125$

### D. Transverse static magnetic fields

We have up until now considered vector potentials of the form $\mathbf{A}(\mathbf{x}) = \Phi\mathbf{e}_1/L$. These vector potentials

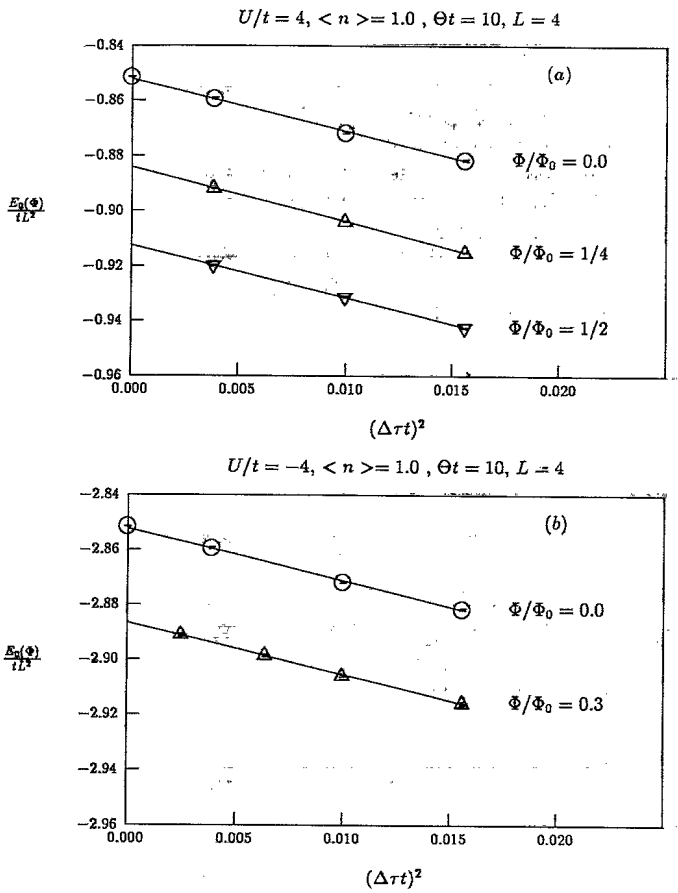


FIG. 3. (a) Ground-state energy of the half-filled repulsive Hubbard model at $U/t = 4$ as a function of $(\Delta\tau t)^2$ for different values of the flux $\Phi/\Phi_0$ ( $\mathbf{A} = \Phi\mathbf{e}_1/L$ ). In all considered cases, the systematic error is proportional to $(\Delta\tau t)^2$. For $\Phi/\Phi_0 = 0$ the data point at $\Delta\tau t = 0$ corresponds to the exact diagonalization result. The solid lines are a least squares fit to the form $A + B(\Delta\tau t)^2$. (b) Same as (a) but for the half-filled attractive Hubbard model at $U/t = -4$. At $\Phi/\Phi_0 = 0$, the half-filled repulsive Hubbard model may be mapped onto the half-filled attractive Hubbard model by carrying out a particle-hole transformation in say the spin-up sector. The data points for the attractive Hubbard model at $\Phi/\Phi_0 = 0$ were obtained from our QMC results for the repulsive Hubbard model and with the use of the above mapping. For values of $\Phi/\Phi_0 \neq 0$ the above mapping is not valid and the data points were calculated from scratch. Note that energy differences at different values of of the flux $\Phi/\Phi_0$ are to a very good approximation independent of $\Delta\tau t$.

just twist the $\mathbf{e}_1$ boundary condition by a phase factor $\exp(2\pi i\Phi/\Phi_0)$. Hence, for the considered models, both $K$ and $V$ are simultaneously real representable in Fourier space. In the previous sections, we greatly benefited from this fact. Here, we wish to consider a model where the relevant operators are not necessarily simultaneously real representable. The model consists of spinless electrons on a square lattice, in a transverse, static, magnetic field and submitted to a nearest-neighbor repulsive interaction. The Hamiltonian reads

$$H = -t\sum_{\langle \mathbf{i},\mathbf{j}\rangle} c_{\mathbf{i}}^{\dagger} c_{\mathbf{j}} \exp\left(\frac{2\pi i}{\Phi_0}\int_{\mathbf{i}}^{\mathbf{j}} \mathbf{A}d\mathbf{l}\right) + \frac{V_0}{2}\sum_{\langle \mathbf{i},\mathbf{j}\rangle} n_{\mathbf{i}} n_{\mathbf{j}}. \quad (13)$$

Here, $n_{\mathbf{i}} = c_{\mathbf{i}}^{\dagger} c_{\mathbf{i}}$ and in the Landau gauge $\mathbf{A}(\mathbf{x}) = -B(x_2, 0, 0)$ so that $\mathbf{B} = (0, 0, B)$ and the square lattice lies in the $\mathbf{e}_1$, $\mathbf{e}_2$ plane. Since we want to put the system on a torus, we require that

$$c_{\mathbf{i}}^{\dagger} c_{\mathbf{j}} \exp\left(\frac{2\pi i}{\Phi_0}\int_{\mathbf{i}}^{\mathbf{j}} \mathbf{A}d\mathbf{l}\right)$$

$$= c_{\mathbf{i}+\mathbf{L}}^{\dagger} c_{\mathbf{j}+\mathbf{L}} \exp\left(\frac{2\pi i}{\Phi_0}\int_{\mathbf{i}+\mathbf{L}}^{\mathbf{j}+\mathbf{L}} \mathbf{A}d\mathbf{l}\right). \quad (14)$$

Here, $\mathbf{L}$ is a vector with norm equal to the linear length of the square lattice, and is oriented along the $\mathbf{e}_1$ or $\mathbf{e}_2$ direction. By noting that $\mathbf{A}(\mathbf{x}+\mathbf{L})$ may be written in the form $\mathbf{A}(\mathbf{x}+\mathbf{L}) = \mathbf{A}(\mathbf{x}) + \nabla\chi_{\mathbf{L}}(\mathbf{x})$, Eq. (14) may be satisfied by imposing the boundary condition

$$c_{\mathbf{i}+\mathbf{L}}^{\dagger} = \exp\left(\frac{2\pi i}{\Phi_0}\chi_{\mathbf{L}}(\mathbf{i})\right) c_{\mathbf{i}}^{\dagger}. \quad (15)$$

The above boundary conditions are consistent provided that the translations $\mathbf{i} \to \mathbf{i} + L\mathbf{e}_1 \to \mathbf{i} + L\mathbf{e}_1 + L\mathbf{e}_2$ and $\mathbf{i} \to \mathbf{i} + L\mathbf{e}_2 \to \mathbf{i} + L\mathbf{e}_2 + L\mathbf{e}_1$ lead to the same wave function. This requirement leads to the constraint that the total flux traversing the lattice is an integer multiple of the flux quantum.[33,34] The flux traversing an elementary cell may be written as $Ba^2 = \Phi_0 p/q$ where $L^2 p/q$ is an integer. Here, $a$ denotes the lattice constant. The noninteracting part of the Hamiltonian (13) corresponds to the Hofstadter problem.[35]

Figure 4 plots the ground-state energy of the above Hamiltonian as a function of $\Delta\tau$ for three electrons on a $6 \times 6$ lattice, $p/q = 1/6$, $V_0 t = 0.84$, and $\Theta t = 10$.

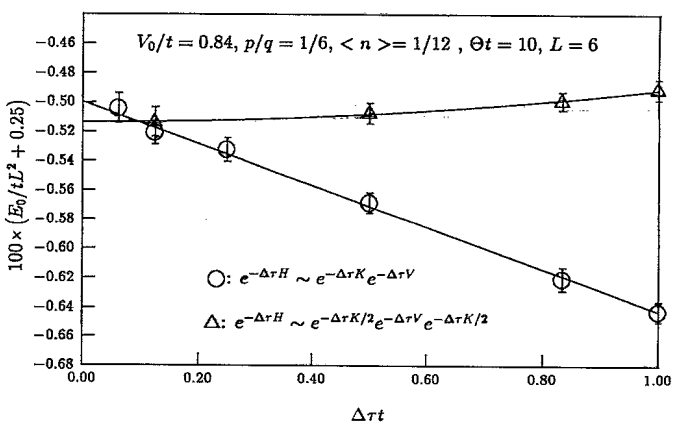


FIG. 4. Ground-state energy for spinless fermions on a square lattice in a transverse magnetic field and submitted to a nearest neighbor repulsive interaction [see Eq. (13)] as a function of $\Delta\tau t$. For both Trotter decompositions, the energy scales to the same $\Delta\tau t = 0$ value within our error bars. For the symmetric Trotter decomposition (16) we fitted the data to the form $A + B(\Delta\tau t)^2$, whereas for the asymmetric decomposition (3), the data was fitted to the form $A + B(\Delta\tau t)$.

One may see that for the Trotter decomposition given in Eq. (3) (circles in Fig. 4), the systematic error is proportional to $\Delta\tau$. According to our previous discussion, $K$ and $V$ are not expected to be simultaneously real representable. However, both the imaginary part of the phase and energy were within our error bars undistinguishable from zero. [Note that by setting the magnetic field to zero, the usual $(\Delta\tau)^2$ behavior of the systematic error was recovered.]

For such situations, it is more convenient to use a higher-order Trotter decomposition given by

$$\left(e^{-\Delta\tau K/2}e^{-\Delta\tau V}e^{-\Delta\tau K/2}\right)^m = e^{-\Theta H} + O((\Delta\tau)^2). \quad (16)$$

Here, $\Delta\tau m = \Theta$ and $H = K + V$. For this decomposition, $B(\Theta) \equiv \left(e^{-\Delta\tau K/2}e^{-\Delta\tau V}e^{-\Delta\tau K/2}\right)^m$ is Hermitian and hence both the average sign and $\langle O\rangle_{\text{approx}}$ [Eq. (4)] are real. One may also note that for finite values of $\Delta\tau$, $\langle H\rangle_{\text{approx}}$ may be written as $\langle H\rangle_{\text{approx}} = \langle\Psi_v|H|\Psi_v\rangle/\langle\Psi_v|\Psi_v\rangle$ where $|\Psi_v\rangle = B(\Phi/2)|\Psi_T\rangle$. Hence, due to the variational principle, $\langle H\rangle_{\text{approx}} \geq \langle\Psi_0|H|\Psi_0\rangle/\langle\Psi_0|\Psi_0\rangle$. Figure 4 plots the ground-state energy as a function of $\Delta\tau$ for the same model and parameters as mentioned above but with the symmetric Trotter decomposition (16) (triangles in Fig. 4). We fitted the QMC data to a $(\Delta\tau)^2$ form as required from Eq. (16). Note the very small dependence of the energy on the considered values of $\Delta\tau$.

Hence, when $K$ and $V$ are not simultaneously real representable, it is more convenient and precise to use the symmetric Trotter decomposition (16). However, algorithms based on the symmetric Trotter (16) decomposition are more expensive in CPU time.

### E. Finite-temperature QMC algorithm

Using the finite-temperature QMC algorithm we can evaluate the internal energy $E(\Phi, T)$ of a given Hamiltonian. In the presence of a magnetic field, this algorithm reacts in exactly the same way as the PQMC approach. Details of the algorithm may be found in Ref. 11. As for the above described PQMC algorithm, and for the models considered here, one may carry out a discrete HS transformation of the interaction term. After integration of the fermionic degrees of freedom, one obtains in the notation of Eq. (7)

$$Z = \text{Tr}e^{-\beta(H-\mu N)} = \sum_{\mathbf{s}} \det M(\mathbf{s}) + O((\Delta\tau)^2),$$

where

$$M(\mathbf{s}) = 1 + \prod_{n=1}^{m}\left(e^{-\Delta\tau T}e^{D(\mathbf{s}_n)}\right). \quad (17)$$

For the PQMC algorithm, $M(\mathbf{s})$ was an $N_p \times N_p$ matrix (7). Here, $M(\mathbf{s})$ denotes is an $N_s \times N_s$ matrix. ($N_s$ is the number of single-particle states; $N_p$ is the number of particles.) We have used the Trotter decomposition (3), since for our application the relevant operators are simultaneously real representable, and thus, the systematic error is proportional to $(\Delta\tau)^2$.[23] For the attractive Hubbard model, $\det M(\mathbf{s})$ factorizes into the product of two identical matrices of dimension $N_s/2 \times N_s/2$. For the repulsive or three-band Hubbard model, $\det M(\mathbf{s})$ factorizes again into two matrices one acting on the spin-up sector and the other on the spin-down sector. From here on our previous discussion of the average phase and $\Delta\tau$ systematic error applies.

In Sec. IV, we will need energy differences for a given average site occupation for different values of the vector potential $\mathbf{A} = \Phi\mathbf{e}_1/L$. A brute force search of the desired chemical potential is numerically too expensive. We thus carried out at least three simulations with chemical potential corresponding approximately to the desired filling and fit the energy data to the form $A + Bx + Cx^2$. The energy corresponding to the desired filling is then extrapolated from the fit. Thus, the calculation of energy differences at given filling and different values of the flux $\Phi$ requires at least six independent simulations.

## III. FLUX QUANTIZATION

In this section, we consider flux quantization[16,17] for the attractive and repulsive Hubbard models. The general aim is to detect superconducting ground states (i.e., zero temperature), without prior knowledge of the underlying symmetry of the pair-pair correlations functions. The setup of the numerical experiment is the following. We thread a flux through a cylinder on which lies the electronic system. From the functional form of the ground-state energy as a function of the threaded flux, $E_0(\Phi)$, one may distinguish between normal and superconducting ground states. As discused in the Introduction, the signature of a superconducting ground states requires (a) $E_0(\Phi)$ to scale to a periodic function of period $\Phi_0/n$ where $n$ denoted the sum of charges in the elementary group (i.e., n=2 for Cooper pairs) and (b) the occurrence of an energy barrier between $\Phi = 0$ and $\Phi = \Phi_0/n$. On the other hand, in the case of a nonsuperconducting ground state, $E_0(\Phi)$ scales to a flat function. Since the above is valid in the thermodynamic limit, our approach is based on the analysis of $E_0(\Phi)$ for lattice sizes up to $10 \times 10$. $E_0(\Phi)$ is calculated with the PQMC (Ref. 8) algorithm described in the previous section for the attractive and repulsive Hubbard models.

The attractive and repulsive Hubbard models we consider are given by

$$H = -t\sum_{\langle\mathbf{i},\mathbf{j}\rangle,\sigma} \tilde{c}^{\dagger}_{\mathbf{i},\sigma}\tilde{c}_{\mathbf{j},\sigma} + U\sum_{\mathbf{i}} n_{\mathbf{i},\uparrow}n_{\mathbf{i},\downarrow}. \quad (18)$$

Here, $\tilde{c}^{\dagger}_{\mathbf{i},\sigma}$ creates an electron with a $z$ component of spin $\sigma$ on lattice site $\mathbf{i}$, $n_{\mathbf{i},\sigma} = \tilde{c}^{\dagger}_{\mathbf{i},\sigma}\tilde{c}_{\mathbf{i},\sigma}$ and the first sum runs over nearest neighbors. Choosing $t\rangle 0$, the attractive (repulsive) Hubbard model corresponds to $U/t\langle 0$ ($U/t\rangle 0$). Since the wave function has to be single valued, a particle going once around the flux line acquires a phase $\exp\left(\frac{2\pi i\Phi}{\Phi_0}\right)$, where $\Phi_0$ is the flux quantum and $\Phi$ the threaded flux.[16] Thus, the fermionic operators are sub-

mitted to the boundary condition

$$\tilde{c}_{\mathbf{i}+L\mathbf{a}_1,\sigma} = \exp\left(\frac{2\pi i\Phi}{\Phi_0}\right)\tilde{c}_{\mathbf{i},\sigma},$$
$$\tilde{c}_{\mathbf{i}+L\mathbf{a}_2,\sigma} = \tilde{c}_{\mathbf{i},\sigma}. \tag{19}$$

Here, $\mathbf{a}_{1,2}$ are the lattice vectors of unit length and $L$ is the linear length of the square lattice. Through a canonical transformation, the Hamiltonian (18) may be written as

$$H(\Phi) = -t\sum_{\mathbf{i},\sigma}\left[\exp\left(\frac{2\pi i\Phi}{L\Phi_0}\right)c^\dagger_{\mathbf{i},\sigma}c_{\mathbf{i}+\mathbf{a}_1,\sigma} + \exp\left(-\frac{2\pi i\Phi}{L\Phi_0}\right)c^\dagger_{\mathbf{i}+\mathbf{a}_1,\sigma}c_{\mathbf{i},\sigma}\right] - t\sum_{\mathbf{i},\sigma}\left(c^\dagger_{\mathbf{i},\sigma}c_{\mathbf{i}+\mathbf{a}_2,\sigma} + c^\dagger_{\mathbf{i}+\mathbf{a}_2,\sigma}c_{\mathbf{i},\sigma}\right)$$
$$+U\sum_{\mathbf{i}} n_{\mathbf{i},\uparrow}n_{\mathbf{i},\downarrow}. \tag{20}$$

The fermionic operators now satisfy periodic boundary conditions in both lattice directions. In the notation of Eq. (1) we have $\mathbf{A} = \Phi\mathbf{e}_1/L$.

In the free case [$U = 0$ in Eq. (20)], the Hamiltonian (20) has a single-particle spectrum of the form

$$\epsilon(\mathbf{k},\Phi) = -2t\left\{\cos\left[\left(n_1 + \frac{\Phi}{\Phi_0}\right)\frac{2\pi}{L}\right] + \cos\left(n_2\frac{2\pi}{L}\right)\right\}, \tag{21}$$

where $n_{1,2}$ are integers included in $-L/2,\ldots,L/2$. For free fermions or bosons of charge 1, the total energy on a finite lattice has a periodicity $E_0(\Phi+\Phi_0) = E_0(\Phi)$. For bosons at $T = 0$, the lowest single-particle state is macroscopically occupied and thus ODLRO is present. In the thermodynamic limit one obtains

$$E_0\left(\frac{\Phi}{\Phi_0}\right) - E_0\left(\frac{\Phi}{\Phi_0} = 1\right) = \begin{cases} 4t\pi^2\rho\left(\frac{\Phi}{\Phi_0}\right)^2, & 0\langle\frac{\Phi}{\Phi_0}\langle 1/2, \\ 4t\pi^2\rho\left(\frac{\Phi}{\Phi_0}-1\right)^2, & 1/2\langle\frac{\Phi}{\Phi_0}\langle 1. \end{cases} \tag{22}$$

Here, $\rho$ denotes the density of particles. Thus, bosons show flux quantization at $T = 0$ [see Fig. 5(b)]. On the other hand, for free fermions, $E_0(\Phi)$ is given by the envelope of a series of energy levels which cross as $\Phi$ is varied. In the thermodynamic limit this envelope becomes flat and thus no flux quantization occurs. The curvature of this envelope at $\Phi = 0$ may be identified to the superfluid density[17,22] [see Fig. 5(a)].

Our analysis is based on the study of

$$\Delta E_0\left(\frac{\Phi}{\Phi_0}\right) = E_0\left(\frac{\Phi}{\Phi_0}\right) - E_0\left(\frac{\Phi}{\Phi_0} = R\right) \tag{23}$$

as a function of lattice size. Here, we will use $R = 0$ or $R = 0.5$. Since $\Delta E_0\left(\frac{\Phi}{\Phi_0}\right) = \Delta E_0\left(1 - \frac{\Phi}{\Phi_0}\right)$, we consider only $0\langle\frac{\Phi}{\Phi_0}\langle 1/2$. We carried out our simulations on $4\times 4$ to $10\times 10$ clusters. For all simulations, we have chosen $\Delta\tau t = 0.125$ and in most cases $\Theta t = 10$. Our calculations carried out with the PQMC algorithm are based on the Trotter decomposition of equation (3).

Figure 6(a) plots $\Delta E_0\left(\frac{\Phi}{\Phi_0}\right)$ for the attractive half-filled Hubbard model at $U/t = -4$. For our large lattice sizes, we were not able to carry out simulations in the range $0\langle\Phi/\Phi_0\langle 1/4$ due to severe phase problems [see Fig. 2(a)]. At strictly half band filling, the attractive Hubbard model shows both long-range superconducting and charge density wave correlations.[36] By carrying out a particle-hole transformation on say the up-spin sector, the attractive, half-filled Hubbard model may be mapped onto the repulsive, half-filled Hubbard model with down spins (up) submitted to a flux $\Phi$ ($-\Phi$). Such boundary

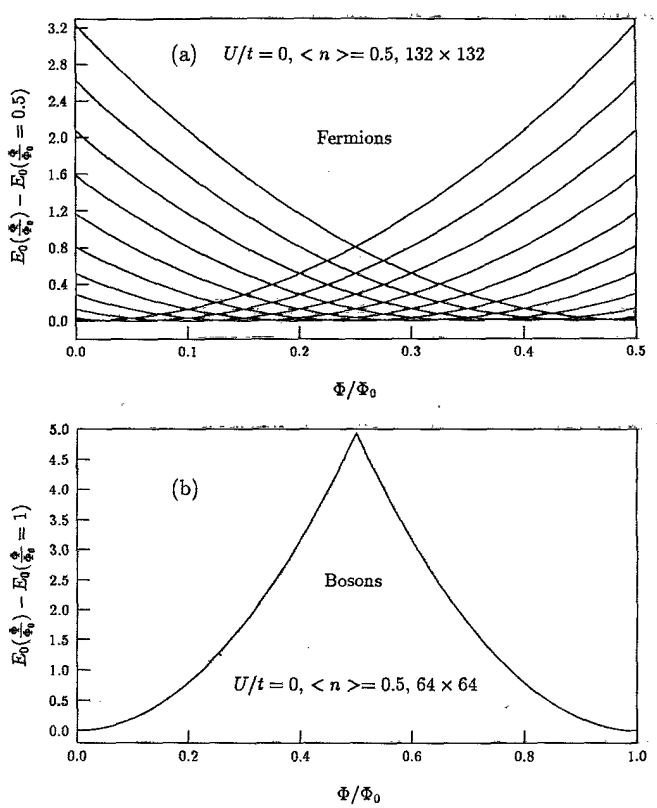


FIG. 5. (a) Example of level crossings as a function of the threaded flux for free fermions on a $132\times 132$ lattice at quarter filling and zero temperature. The envelope of the plotted curves corresponds to the desired $E_0(\Phi/\Phi_0) - E_0(\Phi/\Phi_0 = 0.5)$ function which scales to a flat curve. (b) $E_0(\Phi/\Phi_0) - E_0(\Phi/\Phi_0 = 1)$ for free bosons at zero temperature.

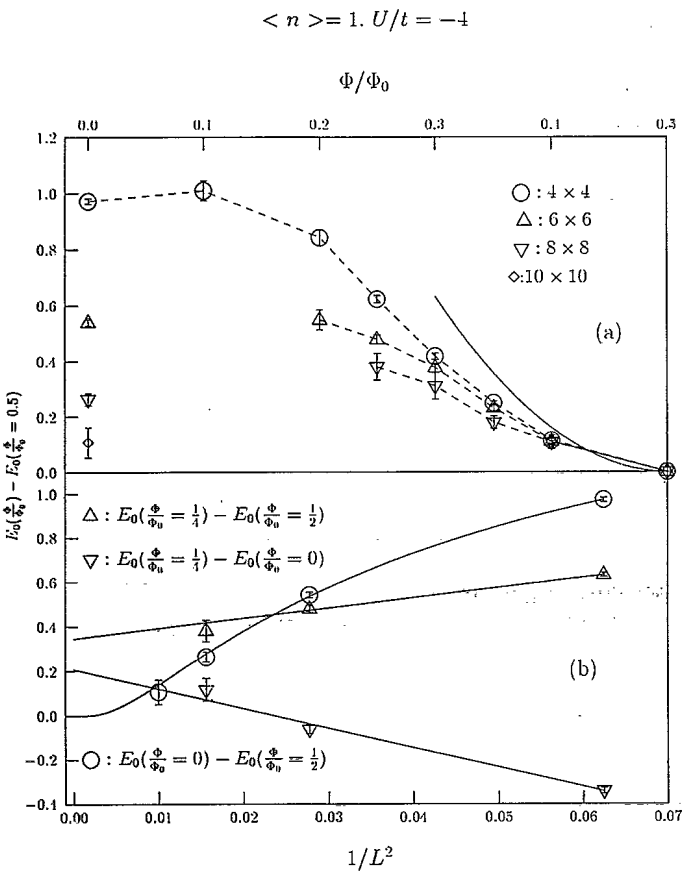


FIG. 6. (a) $E_0(\Phi/\Phi_0) - E_0(\Phi/\Phi_0 = 0.5)$ for the half-filled attractive Hubbard model at $U/t = -4$. The curvature of the plotted parabola (solid line) at $\Phi/\Phi_0 = 0.5$ is obtained from the estimated value of the superfluid density of Ref. 22. The dashed lines are guides to the eye. (b) $\Delta E_1 \equiv E_0(\Phi = \Phi_0/4) - E_0(\Phi = 0)$ (down triangles), $\Delta E_2 \equiv E_0(\Phi = \Phi_0/4) - E_0(\Phi = \Phi_0/2)$ (up triangles), and $\Delta E_3 \equiv E_0(\Phi = 0) - E_0(\Phi = \Phi_0/2)$ (circles) as a function of $1/L^2$ for the half-filled attractive Hubbard model at $U/t = -4$. $\Delta E_1$ and $\Delta E_2$ approximately fit a $1/L^2$ form whereas $\Delta E_3$ was fitted to the form $\Delta E_3 = \Lambda\sqrt{L/\xi}\exp(-L/\xi)$ given in Ref. 21.

conditions have been used by Shastry and Sutherland[37] to measure the spin stiffness of the one-dimensional Hubbard model. In Fig. 6(a), one notes that for values of $1/4 < \frac{\Phi}{\Phi_0} < 1/2$, $\Delta E_0\left(\frac{\Phi}{\Phi_0}\right)$ is very stable against growing lattice sizes. On the other hand, at $\Phi = 0$, $\Delta E_0\left(\frac{\Phi}{\Phi_0}\right)$ decreases very rapidly with growing lattice sizes. The data suggest that $\Delta E_0\left(\frac{\Phi}{\Phi_0}\right)$ converges to a periodic function of period $\frac{\Phi}{\Phi_0} = 1/2$ with a nonvanishing energy barrier at $\Phi = \Phi_0/4$ as appropriate for the condensation of electron pairs. To confirm the above interpretation of the data, we have plotted in Fig. 6(b) the quantities $\Delta E_1 \equiv E_0(\Phi = \Phi_0/4) - E_0(\Phi = 0)$, $\Delta E_2 \equiv E_0(\Phi = \Phi_0/4) - E_0(\Phi = \Phi_0/2)$, and $\Delta E_3 \equiv E_0(\Phi = 0) - E_0(\Phi = \Phi_0/2)$. The existence of a finite-energy barrier at $\Phi/\Phi_0 = 1/2$ requires that both $\Delta E_1$ and $\Delta E_2$ scale to a nonvanishing positive quantity in the thermodynamic limit. This may be seen in Fig. 6(b) where both above mentioned quantities scale to a first approximation as $1/L^2$ to the same nonvanishing value in the thermodynamic limit. On the other hand, and due to the expected periodicity of the $\Delta E_0(\Phi/\Phi_0)$ curve, $\Delta E_3$ should scale to zero. We have fitted in Fig. 6(b) our QMC data for $\Delta E_3$ to the one-dimensional form of Ref. 38 $\Delta E_3 = \Lambda\sqrt{L/\xi}\exp(-L/\xi)$. As may be seen from Fig. 6(b) this form fits equally well our QMC data for the two-dimensional attractive Hubbard model. Hence, we expect in the thermodynamic limit, $E_0(\Phi = 0) = E_0(\Phi = \Phi_0/2)$ and $E_0(\Phi = \Phi_0/4) > E_0(\Phi = 0)$. The superfluid density is related to the curvature of the $\Delta E_0\left(\frac{\Phi}{\Phi_0}\right)$ at $\Phi/\Phi_0 = 1/2$.[39] We may compare our results with those of Scalapino *et al.*[22] The curvature of the parabola plotted in Fig. 6(a) is obtained from Ref. 22, and as may be seen, the agreement to our $\Delta E_0\left(\frac{\Phi}{\Phi_0}\right)$ data is quite good. In contrast, for the repulsive half-filled single-band Hubbard model, the $\Delta E_0\left(\frac{\Phi}{\Phi_0}\right)$ curves scale regularly to zero as a function of lattice size for all values of the threaded flux.[40]

We now consider the quarter-filled attractive Hubbard model at $U/t = -4$. Away from half band filling, the attractive Hubbard model shows long-range superconducting correlations. The charge density wave correlations present at half band filling are now short range.[36] Our results are plotted in Fig. 7(a). As may be seen, the data show no systematic convergence as a function of lattice size. However, for each considered lattice size, clear local flux minima may be found at $\Phi/\Phi_0 = 0$ and $\Phi/\Phi_0 = 0.5$ as expected for a superconducting ground state. Again, the signature of a superconducting ground state requires (1) $\Delta E_0\left(\frac{\Phi}{\Phi_0}\right)$ to scale to a periodic function of period $\Phi/\Phi_0 = 0.5$ and (2) the existence of a finite-energy barrier between $\Phi/\Phi_0 = 0$ and $\Phi/\Phi_0 = 0.5$. Both above mentioned points are hard to detect from the available data. As in Fig. 6(a), we have used the data of Ref. 22 for the superfluid density to obtain the curvature of the plotted parabolas. Both the $6 \times 6$ and $8 \times 8$ lattices show the right curvature at respectively $\Phi/\Phi_0 = 0$ and $\Phi/\Phi_0 = 0.5$. Clearly, the data contain artifacts due to the considered finite-size lattices since, in principle, one should be able to fit the $D_s$ parabolas equally well for the $6 \times 6$ ($8 \times 8$) lattices at $\Phi/\Phi_0 = 0.5$ ($\Phi/\Phi_0 = 0$). As the system size increases, $\Delta E_0(\Phi/\Phi_0 = 1/2)$ should converge to zero. This may not be detected from the data.

Finally, we turn to the quarter-filled repulsive Hubbard model at $U/t = 4$. At the above filling, a phase problem occurs so that only partial results were obtained for the $8 \times 8$ lattice. Our results are plotted in Fig. 7(b). Again, no systematic convergence as a function of lattice size may be seen. However, when one compares the QMC data to a paramagnetic Hartree-Fock (HF) calculation, one clearly sees that for the two largest lattice sizes ($6 \times 6$and$8 \times 8$) the QMC data compare extremely well with the paramagnetic HF prediction of $\Delta E_0\left(\frac{\Phi}{\Phi_0}\right)$. Thus, the data give numerical evidence that the quarter-filled

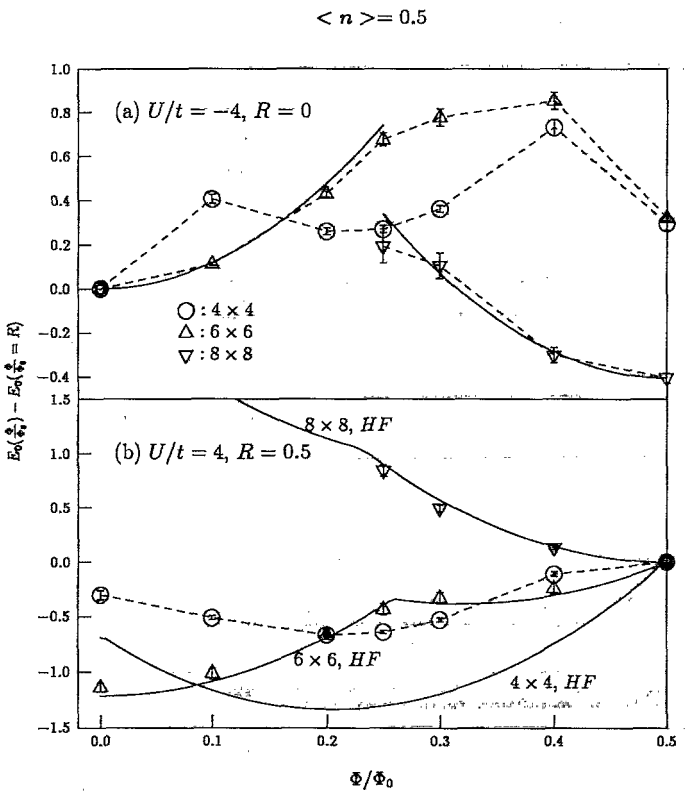


FIG. 7. (a) $E_0(\Phi/\Phi_0) - E_0(\Phi/\Phi_0 = 0)$ for the quarter-filled attractive Hubbard model at $U/t = -4$. Again, the curvatures of the plotted parabolas (solid lines) at $\Phi/\Phi_0 = 0$ and $\Phi/\Phi_0 = 0.5$ are obtained from the estimate of the superfluid density of Ref. 22. The dashed lines are guides to the eye. (b) $E_0(\Phi/\Phi_0) - E_0(\Phi/\Phi_0 = 0.5)$ for the quarter-filled repulsive Hubbard model at $U/t = 4$. The solid lines denote the paramagnetic HF results for the three considered lattice sizes at $T = 0$. The plot symbols represent the QMC data. The dashed line is a guide to the eye.

repulsive Hubbard model has no ODLRO, and that a paramagnetic HF approximation reproduces the QMC data very well.

## IV. TEMPERATURE DERIVATIVE OF THE SUPERFLUID DENSITY

The numerical difficulty in the flux quantization approach described in the previous section lies in the following: (i) Away from half band filling, no systematic convergence as a function of lattice size is found presumably due to level crossing as in the noninteracting case. (ii) Even if the convergence as a function of lattice size is regular, as for the half-filled attractive Hubbard model, the signal we wish to extract is small (i.e., at zero temperature, the potential barrier at $\Phi/\Phi_0 = 1/4$ is an intensive quantity). Here, we wish to present an alternative method which avoids both above mentioned problems. Of course we still have to deal with the phase problem and hope that the KT transition, if present, occurs before the phase problem becomes too severe.

As mentioned in the Introduction, our approach relies on the calculation of the temperature derivative of the superfluid density, $\frac{\partial \beta D_s(\beta)}{\partial \beta}$, where $\beta$ is the inverse temperature. In the framework of a Kosterlitz-Thouless[12] (KT) transition, $D_s(\beta)$ shows a universal jump at the transition temperature.[13] Hence, $\frac{\partial \beta D_s(\beta)}{\partial \beta}$ in the thermodynamic limit behaves like a Dirac $\delta$ function at the transition temperature $T_{\mathrm{KT}}$ and even on finite-sized clusters is expected to yield a very clear signal. Compared to previous estimations of the $T = 0$ superfluid density, via flux quantization described in Sec. III or linear response,[22] the method described here leads to numerical results which exhibit a peak at $T_{\mathrm{KT}}$ which grows as the size of the system increases. This provides a clear signal of the KT transition. Here, we shown that, for the attractive Hubbard model, $\frac{\partial \beta D_s(\beta)}{\partial \beta}$ is given by the difference in internal energy of systems which differ by a phase twist $\pi/2$ in the boundary condition along one lattice direction. The internal energies are extracted from the grand-canonical finite-temperature QMC algorithm on cluster sizes ranging from $4 \times 4$ to $8 \times 8$.

Let us consider the free energy

$$F(\Phi) = -\frac{1}{\beta} \ln \mathrm{Tr} e^{-\beta H(\Phi)}, \tag{24}$$

where $H(\Phi)$ is defined in Eq. (20). Expand it up to second order in $\Phi/\Phi_0$ around $\Phi = 0$. This yields

$$F(\Phi) = F(\Phi = 0) + \left(\frac{\Phi}{\Phi_0}\right)^2 D_s(\beta) + O\left(\left(\frac{\Phi}{\Phi_0}\right)^4\right),$$

where

$$D_s(\beta) = -\left(\frac{2\pi}{L}\right)^2 \left(\langle K_x \rangle + \int_0^\beta d\tau \langle J_x(\tau) J_x(0) \rangle\right),$$

$$J_x = -it \sum_{\mathbf{i},\sigma} \left(c^\dagger_{\mathbf{i},\sigma} c_{\mathbf{i}+\mathbf{a}_x,\sigma} - c^\dagger_{\mathbf{i}+\mathbf{a}_x,\sigma} c_{\mathbf{i},\sigma}\right),$$

$$K_x = -t \sum_{\mathbf{i},\sigma} \left(c^\dagger_{\mathbf{i},\sigma} c_{\mathbf{i}+\mathbf{a}_x,\sigma} + c^\dagger_{\mathbf{i}+\mathbf{a}_x,\sigma} c_{\mathbf{i},\sigma}\right). \tag{25}$$

Here, $D_s(\beta)/2\pi^2$ corresponds to the superfluid density $n_s$ in units where the hopping $t = 1$.[41]

The above equation may be transformed to give

$$\frac{\partial}{\partial \beta}\left[\beta F(\Phi) - \beta F(\Phi = 0)\right] = \left(\frac{\Phi}{\Phi_0}\right)^2 \frac{\partial}{\partial \beta}\left[\beta D_s(\beta)\right] + O\left(\left(\frac{\Phi}{\Phi_0}\right)^4\right). \tag{26}$$

The left hand side of the above equation is just the difference in internal energy: $E(\Phi, T) - E(\Phi = 0, T)$. The right hand side contains the term we are interested in, namely, the temperature derivative of the superfluid density. For an infinite lattice, the jump in the superfluid density at $T_{\mathrm{KT}}$ implies that

$$\frac{\beta \partial D_s(\beta)}{\partial \beta} \sim \delta\left(T - T_{\mathrm{KT}}\right). \tag{27}$$

For a finite-size lattice, the $\delta$-function peak scales as the number of sites $N$.[14]

To determine which values of $\Phi$ are most appropriate for our calculations, we consider the $T = 0$ limit. At zero temperature, we recover the flux quantization approach described in Sec. III. That is,

$$E_0(\Phi) - E_0(\Phi = 0) = \lim_{\beta\to\infty} \lim_{L\to\infty} [F(\Phi) - F(\Phi = 0)] \tag{28}$$

scales in the thermodynamic limit to a periodic function of period $\Phi_0/2$ and a nonvanishing energy barrier is to be seen between the flux minima at $\Phi = 0$ and $\Phi = \Phi_0/2$.[16,17] Thus, the maximal response in $E_0(\Phi) - E_0(\Phi = 0)$ should lie at $\Phi = \Phi_0/4$. The superfluid density, which corresponds to the curvature of the $E_0(\Phi) - E_0(\Phi = 0)$ function at $\Phi = 0$ or $\Phi = \Phi_0/2$,[17,22] may be approximated by

$$\frac{D_s(T=0)}{4^2} \sim E_0(\Phi = \Phi_0/4) - E_0(\Phi = 0) \equiv E_0(\Phi = \Phi_0/4) - E_0(\Phi = \Phi_0/2). \tag{29}$$

The above relations hold for the Bose condensation of free charge two bosons on a square lattice [see Eq. 22]. Numerical evidence for the validity of Eq. (29) for the quarter-filled and half-filled two-dimensional attractive Hubbard models were presented in Sec. III.

Due to the above considerations, we have computed the quantity

$$\Delta E(T) = E(\Phi = \Phi_0/4, T) - E(\Phi = 0, T) \tag{30}$$

as a function of temperature and lattice size. $\Delta E(T)$ yields at finite temperature information on $\frac{\partial \beta D_s(\beta)}{\partial \beta}$ (26) and at $T = 0$ converges for increasing lattice size to the superfluid density (29). As mentioned previously, the internal energies $E(\Phi, T)$ were calculated through the use of the finite-temperature QMC algorithm[9,10] (see Sec. II E).

To illustrate this approach, we consider the attractive Hubbard model at half and three-quarters band filling and $U/t = -4$. Our QMC data are plotted in Fig. 8. At three-quarters band filling ($\langle n \rangle = 0.75$), we were unable to reach inverse temperatures higher than $\beta t = 7$ due to severe phase problems. The data points at $T = 0$ were obtained with the PQMC algorithm. Figure 8 shows a striking difference between the $4 \times 4$ and $8 \times 8$ clusters at $\langle n \rangle = 0.75$. The slope of the $\Delta E(T)$ curves become very large for the $8 \times 8$ cluster size in the temperature region $7 < \beta t < 5$.[42] The available data are compatible with the onset of a Dirac $\delta$-function type response in $\Delta E(T)$ at approximately $T \sim 0.1t$. This temperature value compares favorably with the KT transition temperature obtained from a finite-size scaling analysis of the pair-pair correlation functions.[44] In contrast, such a signal is not obtained at half band filling (see Figs. 8 and Ref. 43).

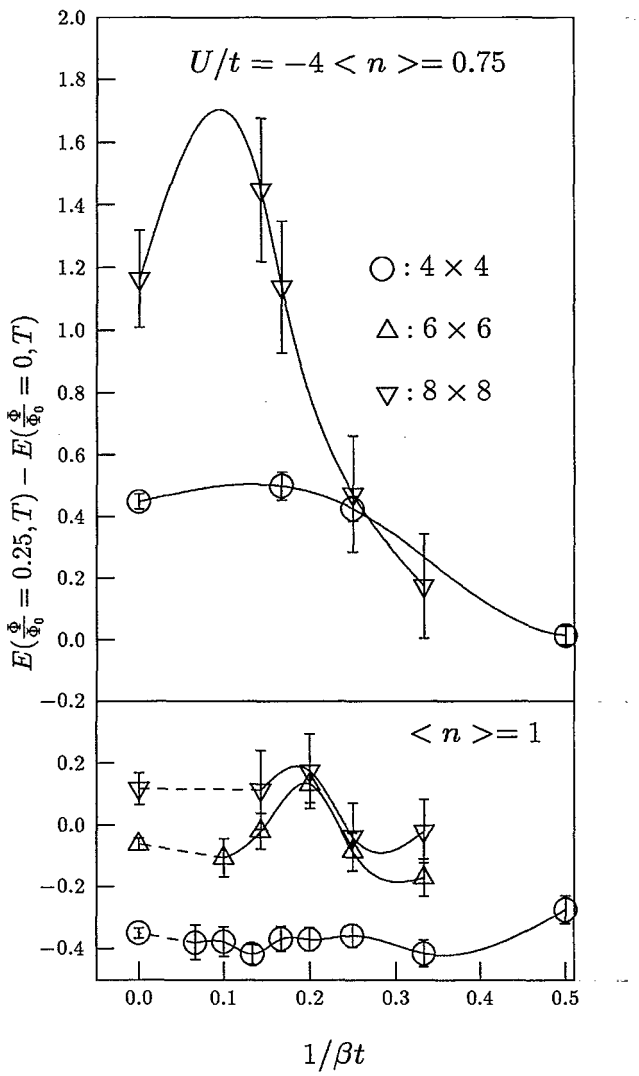


FIG. 8. $E(\Phi = \Phi_0/4, T) - E(\Phi = 0, T)$ as a function of temperature for the half and three-quarters filled attractive Hubbard model at $U/t = -4$. The data points at $T = 0$ were obtained with the PQMC algorithm. The solid lines are spline fits to the data.

## V. THREE-BAND HUBBARD MODEL

We now consider the three-band Hubbard model which takes into account the geometry of the $CuO_2$ planes in high-$T_c$ materials. Following the work of Si *et al.*,[27] we present results for two parameter sets which take into account the difference in Fermi surface as well as the magnetic structure factor between the La-Sr-Cu-O and Y-Ba-Cu-O materials. The three-band Hubbard model we consider is given by

$$H = (\epsilon_d - \mu) \sum_i d_i^\dagger d_i + (\epsilon_p - \mu) \sum_i (p_{x,i}^\dagger p_{x,i} + p_{y,i}^\dagger p_{y,i}) + U_d \sum_i \left[ (d_i^\dagger d_i)^2 - d_i^\dagger d_i \right] + H_{pd} + H_{pp},$$

where

$$H_{pd} = -t_{pd} \sum_{\mathbf{i}} \left[ d^{\dagger}_{\mathbf{i}} (\alpha_1 p_{x,\mathbf{i}} + \alpha_2 p_{y,\mathbf{i}} + \alpha_3 p_{x,\mathbf{i}-\mathbf{a}_x} + \alpha_4 p_{y,\mathbf{i}-\mathbf{a}_y}) + \text{H.c.} \right]$$

$$H_{pp} = -t_{pp} \sum_{\mathbf{i}} \left( \beta_1 p^{\dagger}_{x,\mathbf{i}} p_{y,\mathbf{i}} + \beta_2 p^{\dagger}_{y,\mathbf{i}} p_{x,\mathbf{i}-\mathbf{a}_x} + \beta_3 p^{\dagger}_{x,\mathbf{i}-\mathbf{a}_x} p_{y,\mathbf{i}-\mathbf{a}_y} + \beta_4 p^{\dagger}_{y,\mathbf{i}-\mathbf{a}_y} p_{x,\mathbf{i}} + \text{H.c.} \right)$$

$$-t'_{pp} \sum_{\mathbf{i}} \left( \gamma_1 p^{\dagger}_{x,\mathbf{i}-\mathbf{a}_x} p_{x,\mathbf{i}} + \gamma_2 p^{\dagger}_{y,\mathbf{i}-\mathbf{a}_y} p_{y,\mathbf{i}} + \text{H.c.} \right). \tag{31}$$

Here, $\mathbf{i}$ runs over elementary cells which contain a $d_{x^2-y^2}$ Cu orbital as well as $p_x$ and $p_y$ O orbitals. The Hamiltonian is written in hole notation so that the vacuum consists of filled (with electrons) $d_{x^2-y^2}$, $p_x$ and $p_y$ orbitals. $d^{\dagger}_{\mathbf{i}} = (d^{\dagger}_{\mathbf{i},\uparrow}, d^{\dagger}_{\mathbf{i},\downarrow})$, where $d^{\dagger}_{\mathbf{i},\sigma}$ ($d_{\mathbf{i},\sigma}$) creates (annihilates) a hole with a $z$ component of spin $\sigma$ on the Cu site. The same notation holds for the O orbitals. $\mathbf{a}_x$, $\mathbf{a}_y$ are the lattice vectors of the underlying Cu square lattice and $a = |\mathbf{a}_x| \equiv |\mathbf{a}_y|$. The hopping phases are given by $\alpha_2 = \alpha_3 = 1$, $\alpha_1 = \alpha_4 = -1$, $\beta_1 = \beta_3 = 1$, $\beta_2 = \beta_4 = -1$, and $\gamma_1 = \gamma_2 = -1$. The Hubbard $U_d$ term in (31) is written in spinor form which directly displays the local SU(2) spin invariance. The above Hamiltonian correctly reproduces the geometry of the $CuO_2$ planes of oxide superconductors. The flux is taken into account by imposing the boundary conditions

$$c_{\mathbf{i}+L\mathbf{e}_x} = \exp\left(\frac{2\pi i \Phi}{\Phi_0}\right) c_{\mathbf{i}},$$

$$c_{\mathbf{i}+L\mathbf{e}_y} = c_{\mathbf{i}}, \tag{32}$$

where $c$ denotes a Cu or O spinor and $L$ is the linear length of the square lattice.

For a description of the La-Sr-Cu-O materials, we follow the work of Dopf *et al.*[7,45,46] and choose the parameter set

$$U_d = 6t_{pd},\ \epsilon_p - \epsilon_d \equiv \Delta = 4t_{pd},\ \text{and}\ t_{pp} = t'_{pp} = 0. \tag{33}$$

For this parameter set, the free Fermi surface has for small hole doping a diamond shape form similar to the LDA calculations of Mattheiss.[24] At half band filling, the QMC calculations of Dopf *et al.*[7] show the existence of a charge-transfer gap of the order of $1.2t_{pd}$ and long-range antiferromagnetic correlations.[46] Upon doping incommensurate peaks in the spin structure factor appear along the $(1,0)$ and $(0,1)$ directions in the Brillouin zone appear.[46] This is consistent with neutron experiments on those materials.[28] Besides the magnetic structure, Dopf *et al.*[7] found an attractive interaction in the extended $s$-wave channel which shows a maximum at a hole doping $\delta \sim 0.2$. They also showed that the magnitude of this attractive interaction has not saturated up until inverse temperatures of the order $\beta t_{pd} = 12$. Those results have motivated us to calculate $\Delta E(T)$ [see Eq. (30)] for the above mentioned parameters and at $\delta = 0.25$. As described in Sec. IV the latter quantity gives information on the temperature derivative of the superfluid density. Our results are plotted in Fig. 9(a). We considered a $4\times4$ lattice up to inverse temperature $\beta t_{pd} = 17.5$ and a $6\times6$ lattice up to $\beta t_{pd} = 12.5$. As may be seen from Fig. 9(a) the results show no sign of a KT transition for the considered parameters and temperature regime. Clearly, one may not conclude from the available QMC data that the three-band Hubbard model shows no superconductivity at lower temperatures. Unfortunately, this temperature regime is not accessible to the finite-temperature QMC algorithm due to the phase problem.

For a description of the Y-Ba-Cu-O materials we choose

$$U_d = 6t_{pd},\ \epsilon_p - \epsilon_d \equiv \Delta = 4t_{pd},$$

and

$$t_{pp} = 0.4t_{pd}\ , \text{and}\ t'_{pp} = 0.2t_{pd}. \tag{34}$$

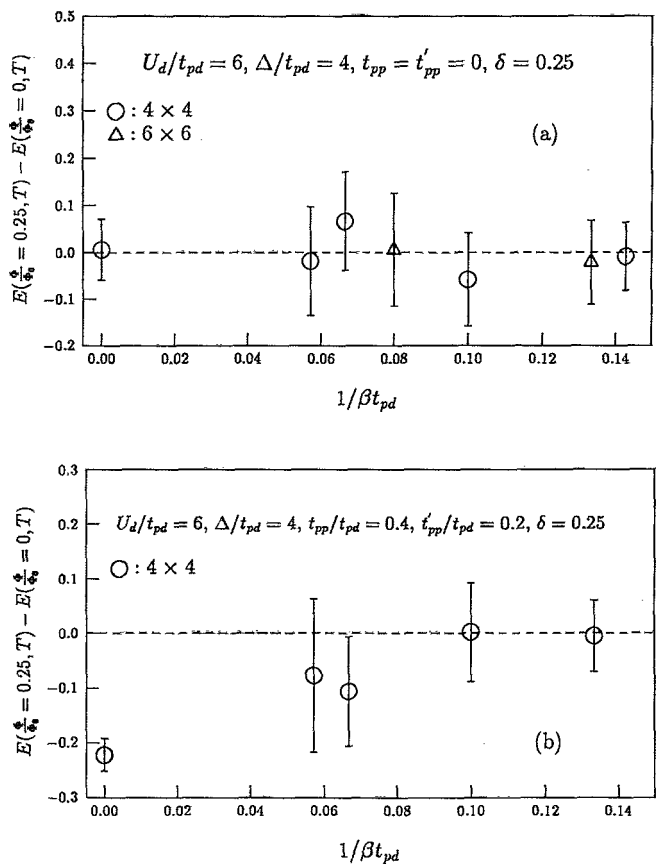


FIG. 9. (a) $E(\Phi = \Phi_0/4, T) - E(\Phi = 0, T)$ as a function of temperature for the three-band Hubbard model at hole doping $\delta = 0.25$. Here, we consider the La-Sr-Cu-O parameters of Eq. (33). The points at $T = 0$ were obtained with the PQMC algorithm. (b) Same as figure (a) but for the Y-Ba-Cu-O parameters of Eq. (34).

For this parameter choice, our QMC simulations yield a charge-transfer gap comparable to that obtained for the above La-Sr-Cu-O parameters. Along with the charge-transfer gap antiferromagnetic order was found at half band filling. Hence, in the half-filled band case, both parameter choice yield the same physics. However, upon hole doping, the magnetic structure factor shows no incommensurate peaks in the $(1,0)$ and $(0,1)$ directions as was the case for the above La-Sr-Cu-O parameters. To be more precise, preliminary QMC simulations carried out on an $8 \times 8$ lattice at hole doping $\delta = 0.218\,75$ show that the spin structure factor shows the same amplitude (within our error bars) for the set of $\mathbf{k}$ points around $\mathbf{k} = (\pi, \pi)$ both in the $(1,0)$ and $(1,1)$ directions [i.e., there is a plateau the the spin structure factor around $\mathbf{k} = (\pi, \pi)$]. Furthermore, a spiral Hartree-Fock approximation similar to that of Ref. 47 shows that upon hole doping the antiferromagnetic state stays energetically favorable for the above Y-Ba-Cu-O parameters. This stands in contrast to the La-Sr-Cu-O parameters where a (1,1) spiral state sets in for any doping away from half band filling.[47] Both above QMC and Hartree-Fock results for the static spin structure factor are consistent with neutron scattering experiments.[29] For our Y-Ba-Cu-O parameters, the free Fermi surface, is more rounded than the 45°-rotated diamond shape of the La-Sr-Cu-O materials.[27,25,48] Note that the LDA Fermi surface of Y-Ba-Cu-O materials corresponds well with experiments.[49] Based on the idea that for our Y-Ba-Cu-O parameters the KT transition temperature, if present, should be higher than for our La-Sr-Cu-O parameter we have calculated $\Delta E(T)$ [see Eq. (30)] on a $4 \times 4$ lattice up to $\beta t_{pd} = 17.5$ and hole doping $\delta = 0.25$. Our results are plotted in Fig. 9(b). As for the La-Sr-Cu-O parameters, no sign of a KT transition was found within the accessible temperature regime.

Due to the failure of the above approach, based on the finite-temperature QMC algorithm, to reach low enough temperatures as well as large lattices, we now turn to the flux quantization method described in Sec. III. The flux quantization calculations are based on the PQMC algorithm described in Sec. II A. For the Y-Ba-Cu-O parameters of Eq. (34), and hole doping $\delta = 0.25$, values of $\Theta t_{pd} \sim 5$ [see Eq. (2)] were found to be sufficient so as to stabilize the ground-state energy within our errorbars.[50] [See for example Fig. 1(b) which plots the ground-state energy as a function of the projection parameter for the attractive Hubbard model. Here, values of $\Theta t = 5$ are just sufficient so as to stabilize the ground-state energy.] As in Sec. III the trial wave function was chosen to be the solution of the noninteracting problem. For values of $\Theta t_{pd} \sim 5$ the average sign (i.e., imaginary part of the phase) was large enough so as to carry out precise simulations.

Figure 10 plots $\Delta E_0\left(\frac{\Phi}{\Phi_0}\right) \equiv E_0\left(\frac{\Phi}{\Phi_0}\right) - E_0\left(\frac{\Phi}{\Phi_0} = 0.5\right)$ [see Eq. (23)] for the Y-Ba-Cu-O parameters of Eq. (34) at hole doping $\delta = 0.25$. Here, we consider $4 \times 4$ and $8 \times 8$ lattices. We have equally plotted for comparison (solid lines in Fig. 10) $\Delta E_0\left(\frac{\Phi}{\Phi_0}\right)$ for $U_d = 0$ and as obtained from a paramagnetic Hartree-Fock approximation. The QMC data of Fig. 10 show no systematic convergence as a function of lattice size and it is instructive to compare it to the results obtained for the quarter-filled attractive and repulsive single-band Hubbard models (see Fig. 7). For the quarter-filled attractive single-band Hubbard model where superconductivity is expected, the QMC data of Fig. 7 showed the existence of local flux minima at $\Phi = 0$ and $\Phi = \Phi_0/2$ for the the three considered lattice sizes. In contrast, the QMC data for the quarter-filled repulsive single-band Hubbard model showed no such flux minima and the QMC data for our two largest lattice sizes were very well reproduced by a paramagnetic Hartree-Fock approximation. Hence, we argued that the latter model did not have a superconducting ground state. With this in mind, let us come back to the three-band Hubbard model. In Fig. 10, the QMC data for the $4 \times 4$ ($8 \times 8$) lattice show a local minima at $\Phi = \Phi_0/2$ ($\Phi = 0$). If flux quantization were present, we would expect another local minima at $\Phi = 0$ ($\Phi = \Phi_0/2$). This is not the case for both considered lattice sizes. On the other hand, the $U_d = 0$ curves reproduce fairly well the QMC data. Note that for the $8 \times 8$ lattice and with the exception of the $\Phi = 0$ data point, the $U_d = 0$ value of $\Delta E_0\left(\frac{\Phi}{\Phi_0}\right)$ is indistinguishable from its QMC value. Hence, the nature of the QMC data of Fig. 10 compares better to the quarter-filled repulsive Hubbard model than to the quarter filled attractive Hubbard model. Similarly to our analysis of the quarter-filled repulsive Hubbard model, we believe that Fig. 10 gives numerical evidence for the absence of a superconducting ground state in the three-band Hubbard model at hole

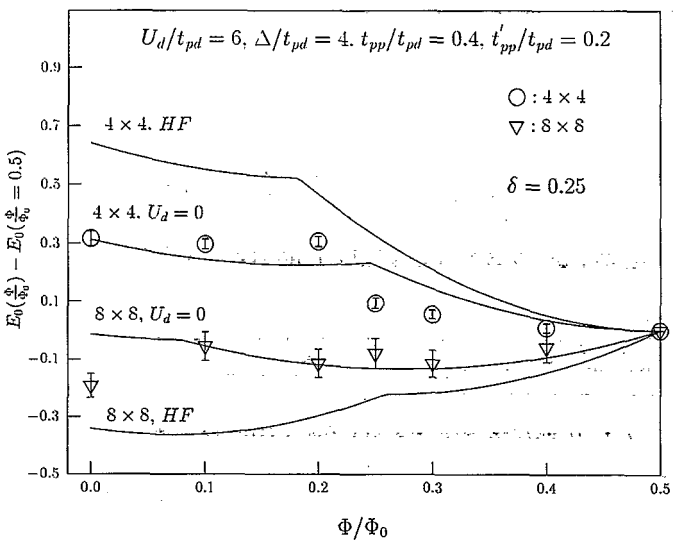


FIG. 10. $\Delta E_0(\Phi/\Phi_0) \equiv E_0(\Phi/\Phi_0) - E_0(\Phi/\Phi_0 = 0.5)$ for the three-band Hubbard model at hole doping $\delta = 0.25$. Here, we consider the Y-Ba-Cu-O parameters given in Eq. (34). The solid lines denoted by HF correspond to a paramagnetic Hartree-Fock calculation of $\Delta E_0(\Phi/\Phi_0)$. The solid lines denoted by $U_d = 0$ correspond to the the value of $\Delta E_0(\Phi/\Phi_0)$ obtained by setting $U_d = 0$.

doping $\delta = 0.25$ and for the Y-Ba-Cu-O parameters of Eq. (34).

## VI. CONCLUSIONS

In this paper, we have presented two methods to detect superconductivity in two-dimensional Hubbard models without prior knowledge of the underlying symmetry and nature of the pair-pair correlation functions. Both methods rely on the extension of the grand-canonical and projector QMC algorithms to incorporate magnetic fields.

The flux quantization approach is a $T = 0$ method based on the PQMC. The basic idea is to reverse the flux quantization experiment for a superconducting *ring* and instead vary the flux $\Phi$ through a cylinder on which lies the electronic system. The existence of a superconducting ground state reflects itself in the existence of metastable states [i.e., minima in $E_0(\Phi)$] at quantized values of the flux $\Phi$. (In BCS theory, local minima are expected at $\Phi = n\Phi_0/2$.) Clearly those local minima are well defined only if they are separated by a potential barrier. On the other hand, a normal ground state (i.e., no ODLRO) shows no flux quantization and hence a flat functional form of $E_0(\Phi)$ is expected. Since the above is valid only in the thermodynamic limit, we have tried to extrapolate the functional form of $E_0(\Phi)$ from QMC calculations on clusters up to $8 \times 8$. In Sec. III we applied this method to the single-band attractive and repulsive Hubbard models. For the attractive half-filled Hubbard model, our data favor the existence of a potential barrier separating local flux minima at $\Phi = n\Phi_0/2$ in the thermodynamic limit. At quarter band filling and for the attractive Hubbard model, no systematic convergence as a function of system size is apparent. Nevertheless, for the three considered lattice sizes, local flux minima are found at $\Phi = n\Phi_0/2$. The QMC data for the quarter-filled repulsive Hubbard model show no local flux minima at $\Phi = n\Phi_0/2$ and are very well reproduced by a paramagnetic Hartree-Fock approximation for our two largest lattice sizes ($6 \times 6$ and $8 \times 8$). Provided that this similarity remains, with growing lattice sizes, our data provide numerical evidence for the absence of superconductivity for quarter-filled repulsive Hubbard model at $U/t = 4$ and zero temperature.

Clearly, the weak point of the flux quantization approach lies in the lack of systematic convergence as a function of lattice size away from half band filling. Even if local minima are found the existence of a potential barrier is very hard to detect. Nevertheless, this criterion has been successfully applied to give convincing arguments against the occurrence of a superconducting ground state. It is to be noted that for the attractive Hubbard model the superfluid density, which we obtain by the curvature of $E_0(\Phi)$ at $\Phi = 0$, compares well to the independent QMC calculations of Scalapino *et al.*[22] In their work, they calculate the finite-temperature linear response of the attractive and repulsive Hubbard models to a transverse magnetic field of wave vector $\mathbf{q}$. By taking the limit $\mathbf{q} \to 0$, they obtain the superfluid density. Hence, both methods are complementary and are plagued by the same difficulties. The major difficulty lies in the sign problem. However, the flux quantization approach requires only the knowledge of ground-state energy which is the most stable and reliable quantity obtained by QMC methods. This allows us to carry out precise simulations up to average signs of the order of 0.1. However, since our information is obtained through total energy differences at different values of the flux $\Phi$, the raw data have to be very precise. As argued Sec. II energy differences at different values of $\Phi$ are to a good approximation not plagued by systematic errors due to the finite imaginary time step $\Delta\tau$.

The other method we presented was based on the calculation of the temperature derivative of the superfluid density, $\frac{\partial \beta D_s(\beta)}{\partial \beta}$. The reason for calculating $\frac{\partial \beta D_s(\beta)}{\partial \beta}$ lies in the fact that in the framework of a KT transition, the superfluid density shows a jump at the transition temperature. Hence, $\frac{\partial \beta D_s(\beta)}{\partial \beta}$ scales in the thermodynamic limit to a Dirac $\delta$ function, and even on small lattices, a signal which grows as the number of sites is expected. Hence, in comparison to the flux quantization approach where we are looking for an intensive signal (i.e., at zero temperature and in the two-dimensional case, the energy barrier between the flux minima is finite), $\frac{\partial \beta D_s(\beta)}{\partial \beta}$ shows an extensive response at $T_{\mathrm{KT}}$ which should be easier to observe. $\frac{\partial \beta D_s(\beta)}{\partial \beta}$ is given by the difference in internal energy of systems which differ by a phase twist $\pi/2$ (i.e., $\Phi = \Phi_0/4$) in the boundary condition along one lattice direction. Since in this approach we fix two values of the flux ($\Phi = 0$ and $\Phi = \Phi_0/4$) we do not encounter level crossings which occur when the flux $\Phi$ is varied. Those level crossings are presumably at the origin of the lack of systematic convergence away from half band filling in the flux quantization approach. In Sec. IV, we applied the method to the three-quarters-filled attractive single-band Hubbard model. Our results give clear evidence of the occurrence of the KT transition away from half band filling. Furthermore the obtained KT transition temperature at $\langle n \rangle = 0.75$ and $U/t = -4$, $T_{\mathrm{KT}} \sim 0.1t$, compares well with the results of Moreo and Scalapino[44] who estimate the transition temperature by carrying out a finite-size scaling analysis of the pair-pair correlation functions.

In Sec. V we considered the three-band Hubbard model which describes the geometry of the underlying $CuO_2$ planes in high-$T_c$ materials. For this model, we considered two parameter sets which take into account some of the differences in Fermi surface and static spin structure factor of Y-Ba-Cu-O and La-Sr-Cu-O materials [see Eqs. (33) and (34)]. Our Y-Ba-Cu-O parameter set was inspired by the work of Ref. 27. At half band filling, both parameter sets yield a comparable charge-transfer gap and long-range antiferromagnetic spin-spin correlations. (For the La-Sr-Cu-O parameter set we refer to the work of Dopf *et al.*[46,7]) However, upon doping, the Y-Ba-Cu-O parameters do not show incommensurate spin structure along the (1,0) directions in the Brillouin zone as was obtained for the La-Sr-Cu-O parameters.[46] For both parameter sets, we calculated the temperature derivative of the superfluid density. In both cases and at hole doping

$\delta = 0.25$, no sign of KT type transition was found in the accessible temperature regime. [For the La-Sr-Cu-O parameters simulations were carried out up to $\beta t_{pd} = 17.5$ ($\beta t_{pd} = 12.5$) on $4\times4$ ($6\times6$) lattices. For the Y-Ba-Cu-O parameters, inverse temperatures up to $\beta t_{pd} = 17.5$ on $4 \times 4$ lattices were reached.] Due to the failure of reaching low enough temperatures within this approach, we carried out $T = 0$ flux quantization calculations for the Y-Ba-Cu-O parameters again at a hole doping $\delta = 0.25$ and for $4 \times 4$ and $8 \times 8$ lattices. Although the data show no systematic convergence, no flux minima were found for either lattice sizes. Furthermore, the QMC data were to a certain extent comparable to the $U_d = 0$ prediction of $\Delta E_0(\Phi/\Phi_0)$. Based on these observations, we argued that the three-band Hubbard model for the Y-Ba-Cu-O parameter set of Eq. (34) and a hole doping $\delta = 0.25$ does not have a superconducting ground state. The occurrence of superconductivity at lower hole doping remains an open question.

## ACKNOWLEDGMENTS

We are indebted to A. Muramatsu for many stimulating conversations and for calling our attention to the necessity of different parameter sets for Y-Ba-Cu-O and La-Sr-Cu-O materials. We would like to thank S. Biskamp, H. Endres, J. Deisz, C. Kübert, W. v. d. Linden, A. Moreo, E. Dagotto, R. Scharf, J. Stein, and A. Sudbø for instructive conversations. F.F. Assaad would like to thank the DFG for financial support under Grant No. Ha 1537/6-1, W.H. the financial support of the Bavarian "FORSUPRA" program on high-$T_c$ research, and D.J.S. financial support from the NSF under Grant No. DMR92-25027. The calculations were performed on the Cray YMP of the HLRZ-Jülich as well as on the Cray YMP of the LRZ-Münich. We have greatly benefited from CPU time obtained at the LRZ-Münich under a cooperation program with Cray Research Inc.

* Present address: ISSP, The University of Tokyo, Roppongi, Minato-ku, Tokyo 106.

[1] P.W. Anderson, Science **235**, 1196 (1987).
[2] V.J. Emery, Phys. Rev. Lett. **58**, 2794 (1987).
[3] C. Gross, R. Joynt, and T.M. Rice, Z. Phys. B **68**, 425 (1987).
[4] N.E. Bickers, D.J. Scalapino, and S.R. White, Phys. Rev. Lett. **62**, 961 (1989).
[5] S.R. White, D.J. Scalapino, R.L. Sugar, N.E. Bickers, and R.T. Scalettar, Phys. Rev. B **39**, 839 (1989).
[6] M. Imada and Y. Hatsugai, J. Phys. Soc. Jpn. **58**, 3752 (1989).
[7] G. Dopf, A. Muramatsu, and W. Hanke, Phys. Rev. Lett. **68**, 353 (1992).
[8] G. Sugiyama and S.E. Koonin, Ann. Phys. (N.Y). **168**, 1 (1986); S. Sorella, S. Baroni, R. Car, and M. Parrinello, Europhys. Lett. **8**, 663 (1989); S. Sorella, E. Tosatti, S. Baroni, R. Car, and M. Parinello, Int. J. Mod. Phys. B **1**, 993 (1989).
[9] J.E. Hirsch, Phys. Rev. B **31**, 4403 (1985).
[10] S.R. White, D.J. Scalapino, R.L. Sugar, E.Y. Loh, J.E. Gubernatis, and R.T. Scalettar, Phys. Rev. B **40**, 506 (1989).
[11] E. Loh and J. Gubernatis, in *Modern Problems of Condensed Matter Physics*, edited by W. Hanke and Y.V. Kopaev (North-Holland, Amsterdam, 1992), Vol. 32, p. 177.
[12] J.M. Kosterlitz and D.J. Thouless, J. Phys. C **6**, 1181 (1973).
[13] D.R. Nelson and J.M. Kosterlitz, Phys. Rev. Lett. **39**, 1201 (1977).
[14] J.E. Van Himbergen and S. Chakravarty, Phys. Rev. B **23**, 359 (1981).
[15] E. Loh, Jr., D.J. Scalapino, and P.M. Grant, Phys. Rev. B **31**, 4712 (1985).
[16] N. Byers and C.N. Yang, Phys. Rev. Lett. **7**, 46 (1961).
[17] C.N. Yang, Rev. Mod. Phys. **34**, 694 (1962).
[18] F. Bloch, Phys. Rev. **137**, A787 (1965).
[19] J.R. Schrieffer, *Theory of Superconductivity* (Benjamin, New York, 1964).
[20] E. Dagotto and J. Riera, Phys. Rev. Lett. **70**, 682 (1993).
[21] A. Sudbø, C.M. Varma, T. Giamarchi, E.D. Stechel, and R.T. Scalettar, Phys. Rev. Lett. **70**, 978 (1993).
[22] D.J. Scalapino, S.R. White, and S.C. Zhang, Phys. Rev. Lett. **68**, 2830 (1992); Phys. Rev. B **47**, 7995 (1993).
[23] All our discussion on the $\Delta\tau$ systematic error is based on the article of R.M. Fye, Phys. Rev. B **33**, 6271 (1986).
[24] L.F. Mattheiss, Phys. Rev. Lett. **58**, 1028 (1987).
[25] J. Yu, S. Massidda, A.J. Freeman, and D.D. Koeling, Phys. Lett. A **122**, 203 (1987).
[26] W.E. Pickett, Rev. Mod. Phys. **61**, 433 (1989).
[27] Q. Si, Y. Zha, K. Levin, and J.P. Lu, Phys. Rev. B **47**, 9055 (1993).
[28] S.W. Cheong *et al.*, Phys. Rev. Lett. **67**, 1791 (1991); T.E. Mason, G. Aeppli, and H.A. Mook, *ibid.* **68**, 1414 (1992).
[29] J. Rossat-Mignod *et al.*, Physica C **185-189**, 86 (1991).
[30] J.E. Hirsch, Phys. Rev. B **28**, 4059 (1983).
[31] In the presence of the above defined vector potential, the attractive Hubbard model shows a phase problem. If one chooses the same trial wave function for the up- and down-spin sectors, the determinant $\det(M)$ factorizes into the product of two identical determinants: $\det(M) = [\det(\tilde{M})]^2$. In the presence of the vector potential, $\det(\tilde{M})$ is a complex number and a phase problem arises.
[32] Here, we have considered the evaluation of the observable $O$ only on the middle time slice. If $O$ commutes with the Hamiltonian, then one may evaluate $O$ on each time slice. This improves the statistic. One may show that, provided $O$ is measured symmetrically around the middle time slice, the systematic error proportional to $\Delta\tau$ vanishes.
[33] E. Fradkin, *Field Theories of Condensed Matter Systems* (Addison-Wesley, Reading, MA, 1991).
[34] F.D.M. Haldane and E.H. Rezayi, Phys. Rev. B **31**, 2529 (1985).
[35] D.R. Hofstadter, Phys. Rev. B **14**, 2239 (1976).
[36] R.T. Scalettar, E.Y. Loh, J.E. Gubernatis, A. Moreo, S.R. White, D.J. Scalapino, R.L. Sugar, and E. Dagotto, Phys. Rev. Lett. **62**, 1407 (1989).
[37] B.S. Shastry and B. Sutherland, Phys. Rev. Lett. **65**, 243

(1990).
[38] C.A. Stafford, A.S. Millis, and B.S. Shastry, Phys. Rev. B **43**, 13 660 (1991).
[39] In this case one expects $\Delta E_0(\Phi/\Phi_0)$ to scale to a periodic function with period 1/2. Since, furthermore, due to time reversal symmetry one has $\Delta E_0(\Phi/\Phi_0) = \Delta E_0(1-\Phi/\Phi_0)$, the curvature of $\Delta E_0(\Phi/\Phi_0)$ at $\Phi/\Phi_0 = 1/2$ is equal to that at $\Phi/\Phi_0 = 0$.
[40] F.F. Assaad, W. Hanke, and D.J. Scalapino, Phys. Rev. Lett. **71**, 1915 (1993).
[41] Note that to obtain the $T = 0$ superfluid density from the expression for $D_s(\beta)$ in Eq. (25) one should first take the limit $L \to \infty$ and then the limit $\beta \to \infty$. This ordering of the limits removes the ambiguity between the superfluid density and the Drude weight (see also Ref. 22).
[42] An accurate scaling of the peak height as a function of the lattice size is out of reach in the present approach due to the phase problem we encounter for values of $\Phi = \Phi_0/4$. At $\langle n \rangle = 0.75$, we did not consider the $6 \times 6$ lattice since for this lattice size $\langle n \rangle = 0.75$ does not correspond to a well-defined particle number in the $S_z = 0$ Hilbert space. Hence, the PQMC algorithm may not be unambiguously applied to obtain the $T = 0$ data point.
[43] F.F. Assaad, W. Hanke, and D.J. Scalapino, Phys. Rev. B **49**, 4327 (1994).
[44] A. Moreo and D.J. Scalapino, Phys. Rev. Lett. **66**, 946 (1991).
[45] G. Dopf, J. Wagner, P. Dieterich, A. Muramatsu, and W. Hanke, Phys. Rev. Lett. **68**, 2082 (1992).
[46] G. Dopf, A. Muramatsu, and W. Hanke, Europhys. Lett. **17**, 559 (1992).
[47] F.F. Assaad, Phys. Rev. B **47**, 7910 (1993).
[48] In order to obtain a more precise fit to the LDA Fermi surface for Y-Ba-Cu-O materials, one should choose $t_{pp} = 0.7t_{pd}$ and $t'_{pp} = 0.5t_{pd}$. However, for these hopping matrix elements, $U_d = 6t_{pd}$, and $\Delta = 4t_{pd}$ QMC calculations show that the charge-transfer gap as well as the antiferromagnetic ordering vanishes at half band filling.
[49] R. Lui *et al.*, Phys. Rev. B **45**, 5614 (1992).
[50] For the $4 \times 4$ lattice we obtained, $E_0(\Phi = 0) = -5.898 \pm 0.013$ at $\Theta t = 5$, $E_0(\Phi = 0) = -5.889 \pm 0.016$ at $\Theta t = 10$, $E_0(\Phi = \Phi_0/4) = -6.108 \pm 0.006$ at $\Theta t = 5$, and $E_0(\Phi = \Phi_0/4) = -6.112 \pm 0.009$ at $\Theta t = 10$. Hence, for both considered values of $\Phi$ the ground-state energy is stabilized already at $\Theta t = 5$. Similarly, for the $8 \times 8$ lattice, we obtained $E_0(\Phi = \Phi_0/2) = -24.096 \pm 0.019$ at $\Theta t = 5$, $E_0(\Phi = \Phi_0/2) = -24.061 \pm 0.033$ at $\Theta t = 6.25$, $E_0(\Phi = 0) = -24.293 \pm 0.02$ at $\Theta t = 5$, and $E_0(\Phi = 0) = -24.307 \pm 0.04$ at $\Theta t = 6.25$. Those numbers equally point out that within our error bars $E_0(\Phi)$ is stabilized already at $\Theta t = 5$.